This is to certify that the
thesis entitled

AUTOMATED COMPENSATION AND CLASSIFICATION
ALGORITHMS FOR ARRAY PROBE EDDY CURRENT
NONDESTRUCTIVE EVALUATION

presented by

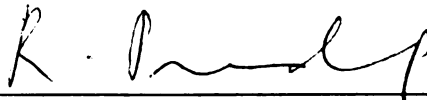PRADEEP KUMAR JELLA

has been accepted towards fulfillment
of the requirements for the

MASTER OF   degree in   ELECTRICAL AND
SCIENCE   COMPUTER ENGINEERING

Major Professor's Signature

12 / 17 / 04

Date

PLACE IN RETURN BOX to remove this checkout from your record.
TO AVOID FINES return on or before date due.
MAY BE RECALLED with earlier due date if requested.

DATE DUE	DATE DUE	DATE DUE

AUTOMATED COMPENSATION AND CLASSIFICATION ALGORITHMS FOR ARRAY PROBE EDDY CURRENT NONDESTRUCTIVE EVALUATION

By

Pradeep Kumar Jella

A THESIS

Submitted to
Michigan State University
in partial fulfillment of the requirements
for the degree of

MASTER OF SCIENCE

Electrical and Computer Engineering

2004

ABSTRACT

AUTOMATED COMPENSATION AND CLASSIFICATION ALGORITHMS FOR ARRAY PROBE EDDY CURRENT NONDESTRUCTIVE EVALUATION

By

Pradeep Kumar Jella

Nondestructive evaluation (NDE) deals with the inspection of an object for determining its properties without destroying its usefulness. Applications include detection of cracking in steam generator tubing in nuclear power plants, aircrafts, etc. Eddy current NDE is one of the more commonly used techniques. This thesis focuses on the problem of multifrequency eddy current inspection of steam generator tubing. Specifically, the thesis examines the use of array probes in the steam generator inspection.

This thesis deals with the development of analysis algorithms for processing of eddy current data collected using array probes from steam generator tubes to detect various types of degradation. The thesis describes compensation algorithms for the effect of probe liftoff in array probe signals, and other signal processing techniques for enhancing the information content in the data. Lift-off compensation is achieved using various techniques including affine transformations and neural networks, which use both single and multi-frequency data. In addition, techniques including the continuous wavelet transform, mixing and classification algorithms are investigated to detect and classify degradation mechanisms. The algorithms developed as part of this thesis were validated on data generated using a numerical model, as well as data obtained by inspection of tubing from in-service steam generators. Results on these data sets indicate the ability of the algorithms for rapid and accurate analysis of array probe eddy current data.

ACKNOWLEDGEMENTS

TABLE OF CONTENTS

LIST OF TABLES

LIST OF FIGURES

CHAPTER 1. INTRODUCTION

Nondestructive testing involves the examination of a material to determine its state without impairing its usefulness. Applications of NDT include finding the presence of flaws in materials, as well as determining whether materials are within specified tolerance levels.

A general NDT system is shown in Figure 1.1 [1]. A transmitter is used to couple energy to the test sample from an energy source. A receiving transducer picks up energy after its interaction with the test object. The signal from the receiver is applied to a series of signal and image processing algorithms that enhance the signal to noise ratio and determine the presence or absence of flaws. Classification algorithms are used to further refine the decision and determine the type of flaw. Finally, defect characterization algorithms are used to determine the parameters, including the defect dimensions and three dimensional shape or profile.
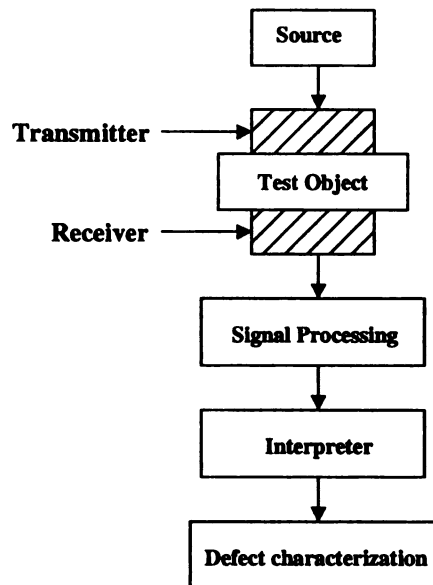
Figure 1.1 A general NDT system (adapted from [1])

1.1 General Methods of Nondestructive Testing

A variety of nondestructive methods are used currently depending on the application and the type of energy source used. Some of the important methods are ultrasonic, magnetic flux leakage, radiographic, penetrant and eddy current techniques. A brief introduction to these methods follows.

1.1.1 Ultrasonic NDT

Ultrasonic inspection can be used for flaw detection/evaluation, dimensional measurements, material characterization etc. Ultrasonic inspection is based on the principle that solid materials are good conductors of sound waves. Therefore any waves reflected are by interfaces or internal material dislocations. The material and sound interaction becomes stronger with smaller wavelength, corresponding to higher frequencies. Therefore, in ultrasonic testing (UT), the frequency of operation is usually greater than 20 kHz and the wavelength is of the order of millimeters. At low frequencies, the interaction between the wave and flaws is minimal making detection of flaws difficult [2].

The transducer used in ultrasonic NDE is usually a piezoelectric element excited by an extremely short electrical discharge, to generate an ultrasonic pulse. It also generates an electrical signal when it receives an ultrasonic signal. Typically, the probe is coupled to the test material by air or through a coupling gel or water to minimize attenuation and back scattering at the probe-material interface, and the object is scanned by evenly moving the probe over the surface. Sound energy propagates through the materials in the form of waves, and when discontinuities (such as a crack) are encountered in the wave path, part of the energy is reflected back. Sound waves reflected

2
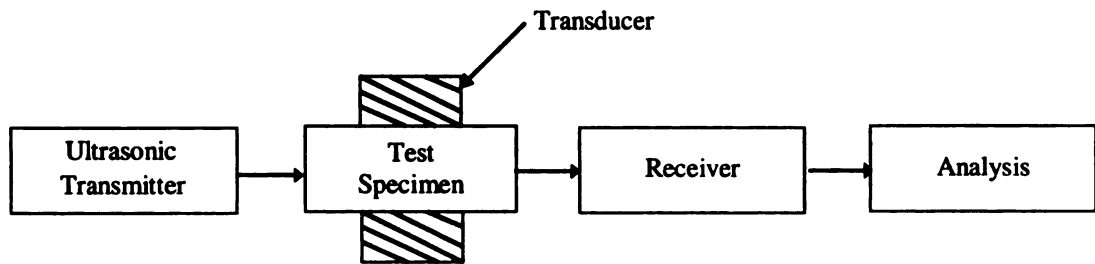
Figure 1.2: Ultrasonic inspection system

in the direction of the transducer due to discontinuities in the object are used for detection

of the flaw.

The reflected wave signal is transformed into an electrical signal by the transducer

and is used to obtain information about reflector location, size, orientation and other

features.

The advantages of ultrasonic inspection include sensitivity to both surface and

subsurface discontinuities, superior depth of penetration when compared to other

methods, higher accuracy in determining the position, size, and shape of defect and

minimal test object preparation. As with all NDT methods, ultrasonic inspection also has

its limitations. Materials that are rough, irregular, very small and thin or not homogenous

are difficult to inspect. Defects oriented parallel to the sound beam may be undetected.

Accessibility of the surface for inspection is also an issue. Finally, the skills and training

required is more extensive compared to other methods.

1.1.2 Radiographic NDE

In radiographic inspection, energy from a source such as X-rays propagates

through a test specimen and the pattern of the energy received on the opposite side is

evaluated. Once radiation passes through the object, an image is projected on the receiver

or recording plane on the opposite side. If there is a considerable difference in the

3

intensities recorded by the film under the defect and rest of the material, then there will

be an image of the defect on the film [1, 3]. All abnormalities in the test object are

viewed on the recording plane as light or dark spots compared to the rest of the material

depending on the properties of the material.

Radiography was the one of the first NDT methods used for inspecting test

objects for internal defects. It is widely used for finding volumetric flaws such as

porosity. However, planar defects can be located with radiography if they are properly

oriented. It can also be used for detecting changes in material composition, thickness

measurement, and locating defective components that cannot be seen in assembled parts.

Figure 1.3 shows a typical radiographic inspection system. The radiation source used can

be X–rays or gamma rays [1] which emit energy that travels in straight lines and

penetrate the test specimen. Both sources are electromagnetic radiation with wavelength

of the order of 10^{-7} to 10^{-11} cm. Because of the high energy level, the radiation has high
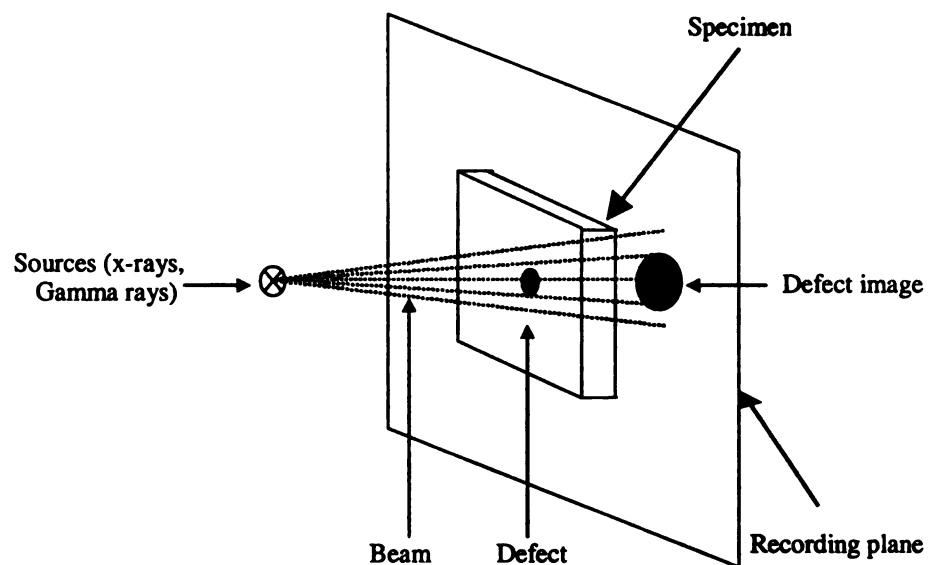
Figure 1.3: A general radiographic NDT system [1]

4

penetrating power and can travel through most materials. The intensity of the beam of energy transmitted through the object is reduced according to the thickness traversed by the beam. The condition of the test object is analyzed by studying the recording obtained on the opposite side.

1.1.3 Penetrant Techniques

Penetrant techniques can be used for detecting surface-breaking defects when large surface areas are involved. Penetrant inspection uses the accumulation of fluid in a material indicating a crack. After accumulation of the penetrant, a developer is used to lift the penetrant out from the flaws [4]. Irregular deformations can be inspected conveniently with penetrant techniques. It may be performed on a variety of materials. One of the most critical steps of a liquid penetrant inspection is surface preparation. The surface must be free of oil, grease, water, or other contaminants that may prevent penetrant from entering flaws. The sample may also require etching if mechanical operations such as machining, sanding, or grit blasting have been performed. These and other mechanical operations can smear the surface of the sample, thus closing the defects. Once the surface has been thoroughly cleaned and dried, the penetrant material is applied by spraying, brushing, or immersing the parts in a penetrant bath. The penetrant is left on the surface for a sufficient time to allow as much penetrant as possible to be drawn from or to seep into a defect.

Penetrant dwell time is the total time that the penetrant is in contact with the part surface. The times vary depending on the application, penetrant materials used, the form of the material being inspected, and the type of defect being inspected. Minimum dwell times typically range from 5 to 60 minutes. The ideal dwell time is often determined by

experimentation and is often very specific to a particular application. This is the most delicate part of the inspection procedure because excess penetrant must be removed from the surface of the sample while removing as little penetrant as possible from defects. Depending on the penetrant system used, this step may involve cleaning with a solvent, direct rinsing with water, or first treating with an emulsifier and then rinsing with water.

A thin layer of developer is then applied to the sample to draw penetrant trapped in flaws back to the surface where it will be visible. Developers come in a variety of forms that may be applied by dusting (dry powdered), dipping, or spraying (wet developers). The developer is allowed to stand on the part surface for a period of time sufficient to permit the extraction of the trapped penetrant out of any surface flaws. This development time is usually a minimum of 10 minutes and significantly longer times may be necessary for tight cracks. Inspection is then performed under appropriate lighting to detect indications from any flaws which may be present. The final step in the process is to thoroughly clean the part surface to remove the developer from parts that were found to be acceptable.

1.1.4 Eddy Current Techniques

Eddy current testing is an electromagnetic technique used to inspect electrically conducting materials for discontinuities, irregularities in structure, etc. Eddy current testing can be used to inspect non-magnetic but conducting materials [3, 5]. Eddy currents can be used to extract information on the local electrical conductivity of various materials, which is a function of mechanical and chemical properties [6]. Different kinds of eddy current probes can be used to scan the test sample. A scanning procedure has to be followed for each type of probe to obtain meaningful information from the test. A

coil carrying alternating current generates an alternating magnetic field that is parallel to the coil's axis. This causes induced currents in the test material in close proximity to the coil according to Faraday's laws. A secondary magnetic field is generated due to the presence of eddy currents in the specimen. In the presence of a defect or discontinuity, the induced current changes, and is reduced due to the presence of the flaw. As a result the impedance of the test coil changes when it is near the conducting material. Therefore systems capable of detecting changes in the impedance of coils can be used to detect flaws.

Various factors like electrical conductivity, magnetic permeability, frequency, lift-off, probe design etc. can affect the coil impedance in an eddy current system [7]. Eddy current testing is dealt with in greater detail in the next chapter.

Some of the advantages of eddy current inspection are its sensitivity to small cracks, detection of surface and near-surface defects. Eddy current testing (ECT) gives
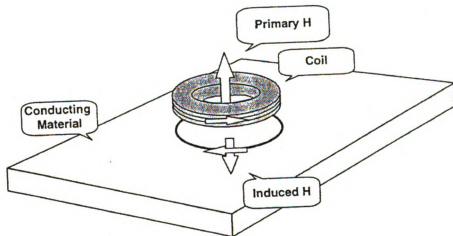
Figure 1.4 Principles of eddy current testing [7]

instant results from inspections and the equipment is portable. Minimal test object preparation is needed for eddy current inspection. The probe used need not contact the test object, and complex objects can be inspected.

Some of the limitations of eddy current inspection are limited depth of penetration and the fact that testing is limited to conductive materials. The surface to be inspected must be close to the probe and the skill and training required for operators is extensive. Surface roughness may interfere in inspection and reference standards should be setup. Furthermore, flaws parallel to coil winding and scan direction may be undetected.

1.2 NDE Applications

NDE is used in a wide range of industries, including nuclear power, aerospace, medical and energy industries. In addition, the application of NDE technologies is increasingly being used in quality control applications for online monitoring of processes. The NDT industry is continually changing as the technologies are evolving, as are applications. Several examples are presented below.

1.2.1 Aerospace Industry

Over the past few decades, aircraft design and maintenance underwent revolutionary changes. The life-time of an aircraft can typically be 25 to 40 years, while the development of new materials and their introduction into structures can take 10-20 years [8]. Once an aircraft enters service, aging effects are caused by the flight environment, fatigue and operational extremes, and anomalies occur in the aircraft. Therefore NDT methods are essential in the aerospace industry. However, the NDT community that supports the aerospace industry faces a variety of challenges, including the evaluation of newer aerospace structures and materials, and in-service inspection and

monitoring of aging aircraft [9]. Instead of finding a problem or damage found in aircraft and fixing it, the aerospace industry predicts and manages the damage. The damage is predicted using models, with NDT support over a period of time. The damaged structure is fixed or replaced only when the damage reaches a threshold. These changes would not have existed if suitable NDT methods have not been developed. In the past, little thought was given to the design of aircraft components and the provision of suitable access to components with respect to accomplishment of NDT. New steps are now taken by manufacturers to accomplish NDT. NDT is used in airframe manufacture, engine manufacture, aircraft materials and aircraft wiring.

1.2.2 Medical Industry

In addition to industrial applications of NDE to flaw detection, these methods are also used in noninvasive diagnostics and treatment of many disorders in humans and animals. Nondestructive evaluation plays a major role in the medical industry. Techniques such as visual and acoustic methods were prevalent for a long time. New imaging techniques like MRI, electromagnetics and ultrasonics have made a strong contribution in the medical field [10]. Physicians today have a wide range of options to choose from, and instruments today can obtain images with high sensitivity and resolution to the extent of even monitoring the movements of a fetal heartbeat and measurements of blood flow in fetal blood vessels. Real-time and 3-D imaging techniques have added powerful imaging capability, better interpretation, and its presentation to patients. Many diseases can be detected at an early stage and this significantly increases the chances for patient recovery. Nondestructive or noninvasive tools have become indispensable in medical diagnostic applications. Medical

applications include imaging for abdominal and obstetrics for tumors and fractures. Breast cancer detection is also a major application, where tumors need to be detected [10].

1.2.3 Energy Industry

Nondestructive testing finds its place in the energy industry in a variety of applications such as examining thick walled pressure vessels, boilers, steam piping, turbines, nuclear fuel storage and waste containment and heat exchangers. Other applications include inspection of coating for wear and corrosion resistance, welds, power generation, turbine rotors and shafts, fuel storage containers, critical valve testing, testing under insulation etc. Energy applications need both reliable and cost-effective nondestructive solutions which provide invaluable information about the system's condition and lifetime prediction. Suitable NDT methods for each of the applications are necessary for online inspection, which have the ability to locate damage at a significant distance from the sensor and offer reduced inspection costs and improved probability of detection. Many methods monitor the various energy applications continuously. NDE provides many benefits like improved methodologies for condition assessment and subsequent reliability. In today's environment, life extensions for energy related systems are pursued aggressively, and material degradation determines the useful life of the system.

1.3 Steam Generators in Nuclear Power Plants

Steam generators are heat exchangers in nuclear power plants used to transfer heat from the primary to the secondary side of the reactor. It is important that radioactive coolant present in the primary side does not leak out. The tubes are continually exposed

to harsh environmental conditions, such as very high temperatures and pressures. These conditions cause different kinds of degradations to occur at different locations in the tubes. The detection of these defects in a timely fashion is necessary since prolonged exposure to harsh conditions can result in failure of the tube, and consequent leakage of the radioactive coolant to the secondary side. Thus, there is a need for periodic inspection of steam generator tubing. Currently, both eddy current and ultrasound techniques are used extensively for the inspection of steam generator tubes.

Multifrequency eddy current systems with different probe designs are used to collect data to detect flaws and investigate tube conditions. Bobbin probes and rotating probes have been in used in the industry in the past and have produced reasonable detection results. A third type of probe, the array probe is currently being investigated for steam generator inspection in the industry. The array probe provides the advantages of both bobbin probes (speed) as well as rotating probes (resolution). The array probe is relatively new and its performance and contribution to the detection of flaws is being investigated.

The aim of this thesis is to understand the response of array probe to various types of defects and develop algorithms to enhance detection of degradations using data collected from the array probe.
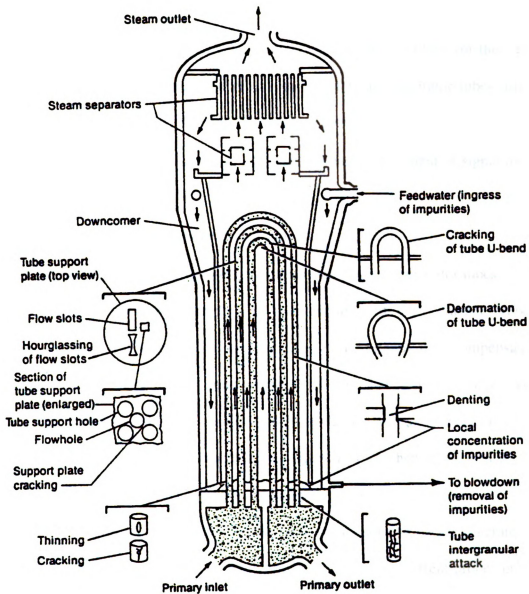
Figure 1.5 Steam generators present in nuclear power plants (adapted from [13])

Steam outlet
Steam separators
Feedwater (ingress of impurities)
Downcomer
Cracking of tube U-bend
Tube support plate (top view)
Flow slots
Hourglassing of flow slots
Deformation of tube U-bend
Section of tube support plate (enlarged)
Tube support hole
Flowhole
Support plate cracking
Denting
Local concentration of impurities
To blowdown (removal of impurities)
Thinning
Cracking
Tube intergranular attack
Primary inlet
Primary outlet

1.4 Scope of Thesis

This thesis focuses on the development of automated algorithms for the analysis of eddy current data obtained during the inspection of steam generator tubes using an array of transmit-receive coils. Algorithms are developed for

- Filtering of low and high frequency noise and the enhancement of signal to noise ratio (SNR)

- Suppression of signals from external support structures

- Automated detection of flaws in various regions of steam generator tubes

A comprehensive understanding of the operation of eddy current probes is necessary for the development and optimization of algorithms that compensate for various factors. We develop 2D finite element models that simulate the inspection process using transmit-receive coils, and use the models to investigate some of the factors that affect the measured signal. Compensation algorithms are then developed for these factors. The rest of this thesis is organized as follows.

The principles of eddy current testing and applications in steam generator tube inspection are described in Chapter 2. The various types of eddy current probes in steam generator inspection, and data collection procedures using these probes are also described. Chapter 3 addresses finite element modeling of a transmit-receive pancake coil configuration. A finite element model for the transmit-receive coils in a steam generator tube is generated and the effect of different parameters like the offset of coils with respect to the flaw center, flaw depth, inner diameter/ outer diameter defects, frequency and probe liftoffs are studied. Results of the modeling are also presented. Algorithms for analyzing array probe eddy current data are discussed in Chapter 4. In addition to flaw

detection algorithms, classification and compensation algorithms are also presented. Chapter 5 presents a discussion of the results and summarizes the performance of the proposed algorithms. Finally Chapter 6 presents a summary of the thesis and draws conclusions.

CHAPTER 2. EDDY CURRENT NDE

Eddy current testing is an NDT method that uses the principle of electromagnetics as the basis for performing inspections. Other methods such as Flux Leakage and Remote Field Testing [10] are also based on the use of electromagnetic theory.

Eddy current testing originated with Faraday's discovery of electromagnetic induction. Later, Hughes recorded changes in the properties of a coil when placed in contact with metals of different conductivity and permeability [10]. However, much work in testing materials was done later, particularly in the nuclear and aerospace industries. Eddy current testing is a widely used inspection technique.

Eddy current testing is used in many applications to find defects and make measurements. One of the basic uses of eddy current inspection is for defect detection when the nature of the flaw is well known. The technique is used to inspect a relatively small area. The probe design and test parameters must be chosen with a good understanding of the flaw that the technique is trying to detect [10]. Since eddy currents concentrate at the surface of a material, they can only be used to detect defects close to the surface.

The eddy current method is also useful in detecting corrosion damage and thinning. The technique is used to make corrosion and thinning measurements on aircrafts and heat exchangers [10]. Eddy currents are affected by the electrical conductivity and magnetic permeability of materials. Therefore, eddy currents can be used to detect materials types and to determine if a material is exposed to high temperatures, since such treatment changes the conductivity of certain materials.

2.1 Principles of Eddy Current Testing

Eddy currents are generated through electromagnetic induction [10]. When alternating current is passed through a conductor, a magnetic field develops around the conductor. This magnetic field increases or decreases based on the change in the alternating current. If another conductor is kept in the close proximity of this field, current will be induced in the second conductor. Eddy currents are induced currents that flow in a circular fashion.

One of the main advantages of the eddy current technique is the variety of inspections and measurements that can be performed. It can be used for crack detection and material thickness measurements. In addition it can be used for conductivity measurements, material identification and depth determination.

As described above, in eddy current testing, a coil is excited with alternating currents, which induce eddy currents in the test object. The interaction of these currents with defects can cause a change in the exciting field. This is detected by measuring a change in impedance of the exciting coil or the pick up coil. As the source moves over a specimen, changes occur in its impedance when it moves over a defect, which carry information like shape, size and location of the defect. The governing equations describing the material interaction are Maxwell's equations and the solution has a closed form for simple problems or with simplifying conditions.

The differential equations governing the general time-varying fields in regions of conducting materials can be derived from the Maxwell equations [5, 11].

We made the following assumptions:

- The media are linear and isotropic.

16

- The medium has no free charge in the solution region. The only electric field in the solution region is due to the exciting current densities.

Then, it is easy to show that [5, 11]

$$\upsilon \nabla \times (\nabla \times \vec{A}) = -\sigma \frac{\partial \vec{A}}{\partial t} - \sigma \nabla \phi \qquad (2.1)$$

$$\nabla^2 \phi = -\frac{\partial}{\partial t}(\nabla \cdot \vec{A}). \qquad (2.2)$$

where

υ is the reluctance

$\vec{A}$ is the magnetic vector potential

$\vec{\sigma}$ is the conductivity in S/m

ϕ is the electrical scalar potential

Eqs. (2.1) and (2.2) are the basic field equations describing the electromagnetic field in linear media [5, 11].

2.2 Skin Effect

Eddy currents are induced currents circulating in loops in planes perpendicular to the magnetic flux. They travel parallel to the coil's winding and their flow is confined to the area of the inducing field. Eddy currents circulate near the surface close to an excitation coil and their strength decreases with increasing distance from the source. Eddy current density also decreases exponentially with depth. This is known as the skin effect. Skin effect occurs when the eddy currents flowing in the test material at any depth produce magnetic fields which oppose the primary field, thus reducing net magnetic flux and causing a decrease in current flow as depth increases [10, 12]. Eddy currents close to

17

the surface can be seen as obstructing the coil's magnetic field, thereby weakening the magnetic field at greater depths.

The frequency of the excitation, electrical conductivity and magnetic permeability of the test material affect the depth of penetration [10, 12]. It decreases with increasing frequency, conductivity and magnetic permeability. The depth at which eddy current density decreases to $\frac{1}{e}$ is called the standard depth of penetration and is given by

$$\delta = \frac{1}{\sqrt{\pi f \mu \sigma}}$$
(2.3)

where

δ = Standard depth of penetration in m

f = Test frequency in H

μ = Magnetic permeability in N/A^2

σ = Electrical conductivity in S/m

Though eddy currents penetrate deeper than one standard depth, the density reduces with
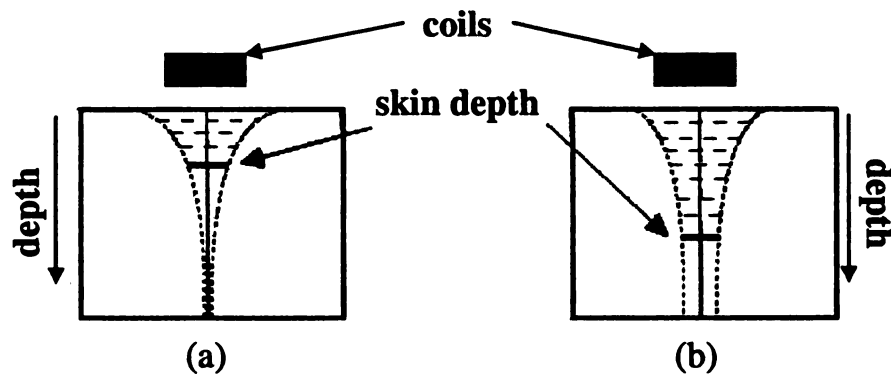
Figure 2.1 Depth of penetration (a) high frequency, conductivity and permeability (b) low frequency, conductivity and permeability (adapted from [10])

18

depth. At 2δ, eddy current density decreases to $\frac{1}{e^2}$. At 3δ, it is reduced to 5% of the original.

Since the sensitivity of the test depends on the eddy current density at the defect location, one must know the strength of the eddy currents at this location. When detecting flaws, a frequency is selected which places the expected flaw depth within one standard depth of penetration [10]. This ensures that the eddy current density will be sufficient to produce a signal from the flaw.

2.3 Eddy Current Probes

Eddy current probes are classified based on their configuration and operation mode. Surface probes, ID (Inner Diameter) probes, and OD (Outer Diameter) probes include some common probes classified on configuration.

Surface probes are used in contact with the test surface and consist of a coil of fine wire encased in a protective case [12]. The coil shape and size are determined by the application. Coils are generally wound such that the inspection surface is perpendicular to the coil axis. This is known as a pancake coil and is excellent for detecting surface defects perpendicular to the test surface. Defects that are parallel to the test surface would not be detected by this configuration.

Wider surface probes are used when scanning larger flaws. They scan a relatively large area and the depth of penetration is higher. However, their large sampling area confines their ability to detect smaller flaws. Pencil probes have a small surface coil that is encased in a long slender case to allow inspection in restricted areas [10, 12]. However, pencil probes are inclined to wobble due to their small base.

ID probes or bobbin probes, are used to inspect hollow products, such as a tube. ID probes have a case that help in keeping the probe centered in the tube and the coil orientation constant relative to the test material. The coils are wound around the circumference of the probe enabling the probe to inspect an area around the entire circumference of the test object at a given time. OD probes, on the other hand, are similar to ID probes except that the coils encircle the material to inspect from the outside. OD probes are used to inspect solid products.

2.3.1 Modes of Operation

Eddy current probes are available in a variety of shapes and sizes to meet different application needs. The mode of operation of these probes refers to the way the coils are wired and interface with the test equipment [10, 12]. Absolute, differential, reflection and hybrid probes are the general classifications based on the mode of operation.

Absolute probes have a single test coil used to generate eddy currents and sense flaw information in test material. An alternating current is passed through the coil, which develops a magnetic field in and around the coil. When the probe is placed close to a conductive material, the changing magnetic field generates eddy currents in the material, which in turn derives energy from the source coil, appearing as an increase in the resistance of the coil. The eddy currents generate their own magnetic field that opposes the source magnetic field, and this changes the reactance of the source coil. By measuring the impedance of the test coil, information can be obtained about the test object.

Absolute coils are used for defect identification, liftoff and thickness measurements. Since absolute probes are sensitive to factors such as conductivity,

20

permeability and liftoff, these variables must be minimized when they are not important to the inspection [10, 12].

Differential probes have two coils wound in opposition. When the two coils pass over an area with no defect, there is no differential signal developed between the coils since they are both inspecting identical material. However, when one coil is over a defect and the other is not, a differential signal is produced [10, 12]. The differential probes are very sensitive to defects and insensitive to slow variations such as expansions. Interpretation of signals can be difficult at times with differential probes. For example, if the length of the defect is longer than the coil spacing, only the leading and trailing edges will be detected due to signal cancellation [10].

Reflection probes have two coils similar to a differential probe, but one coil is used to transmit and the other is used as a receiver. These types of probes are called as transmit-receive probes. In reflection probes, the transmit coil can be made so as to produce a strong and uniform field in the neighborhood of the receiver coil. The receiver coil is made very small so that it will be very sensitive small defects. The use of this probe gives enhanced SNR for detection and is advantageous when deeper penetration is required, such as detection of internal defects. The transmit coil is driven by an oscillator and depending on the configuration, reflection probes can give absolute or differential response. The advantage is that transmit and receive coils can be optimized independently. Such probes also have a wider frequency range than other probes and the larger driver coil gives a more uniform field giving better penetration.

Hybrid probes operate in the reflection mode but its sensing coils operate in the differential mode. This probe is very sensitive to surface cracks. Hybrid probes are specially designed for a specific inspection needs.

2.4 Factors Affecting Eddy Current Signals

The factors that can affect an eddy current signal include the coil spacing in transmit and receive coils and offset with respect to the flaw center. Flaw orientation and flaw depth also play a major role in the contribution to the eddy current signal. ID/OD (Inner Diameter/ Outer Diameter) effects, permeability, excitation frequency and liftoff are other important parameters that can affect the eddy current signal in inspection systems.

Eddy current inspections can be performed at single and multiple frequencies. In multiple frequency eddy current testing, data is collected at several different frequencies. In many applications the test conditions need inspections to be performed at multiple frequencies. Multiple frequency inspections help in acquiring more information from the test and the detection and classification of defects becomes much simpler compared to single frequency examinations. The data is then analyzed and compared at different frequencies. Data fusion and mixing can be performed on data collected at different frequencies.

The impedance of an eddy current probe can also be affected by variations in operating frequency, electrical conductivity, magnetic permeability, structural changes, lift-off, cracks, thinning, denting, supports etc.

Many of these factors exist at the same time. In a simple case of detecting defects, a differential probe can be used to remove unwanted artifacts, if they are varying

gradually. For example, conductivity and temperature variations affect both coils of a differential probe simultaneously. However, if unwanted factors that occur suddenly are affecting the measurements, they can sometimes be suppressed by mixing signals collected at several frequencies. Multi-frequency eddy current technique is commonly used in steam generator tube inspections. The tubing is supported at regular intervals by means of tube support plates. When inspecting the full wall thickness of the tubing, the signal from the support can interfere. By collecting a signal at the frequency necessary to inspect the full thickness of the tube and subtracting a second signal at a different frequency, the support signals can be suppressed.

2.5 Calibration

Calibration is an important step in eddy current inspection. The data collected from the inspection has to be calibrated for accurate defect analysis. Calibration acts as a form of compensation for variable instrument settings and probe variations, thus providing for a simpler comparison between measurements taken at different intervals. The process of calibration also provides for the development of simple calibration curves that map signal characteristics (such as phase angle or amplitude to flaw depth).

The calibration operation requires use of a calibration standard, which is made of the same material as the test specimen. Various defects with dimensions are introduced into the calibration standard and the calibration standard is inspected prior to the test specimen. The calibration operation then generally consists of rotating and scaling of one or more reference flaws on the calibration standard. The parameters obtained by the rotation and scaling of the reference signals on the calibration standard are then applied to the data collected from inspection of the test specimen. Figure 2.2 depicts the rotation of
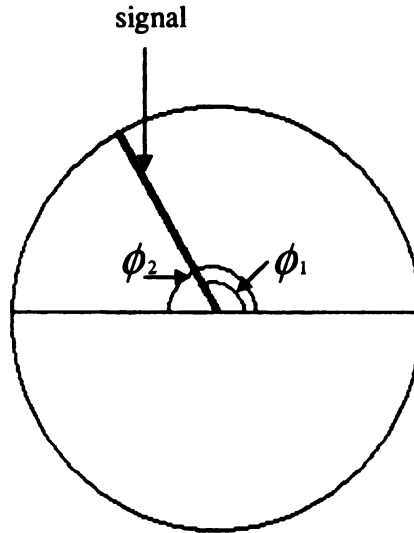
Figure 2.2 Rotation in calibration

a signal. The rotation and scaling parameters are computed as follows. If ϕ_1 is the angle of

the signal and it has to be rotated to an angle ϕ_2, then the rotation angle θ is given by

$$\theta = \phi_2 - \phi_1.$$ (2.4)

The scale factor is determined as

$$s = \frac{r_1}{r_2}.$$ (2.5)

where

S=scale factor

r_1 = desired peak to peak scaling of the signal

r_2 = original peak to peak value of the signal

Eddy current calibration standards are developed with different types of defects to meet

any inspection need today. Typical standards include signals such as grooves, through-

wall holes, EDM (Electrical Discharge Machining) notches, cracks and dents.

24

Reference standards used are manufactured from the same type of material, alloy, material thickness, and chemical composition that will be found on the test component to be inspected. Sizes and tolerances of flaws in the reference standards are usually regulated by inspection specifications.

2.6 Other Factors

In an eddy current test, getting enough eddy current field strength in the region being inspected in the material is a prime issue. Keeping the field away from the irrelevant features of the object is another challenge. Such irrelevant features could produce a response that can interfere with the desired signal. Probe shielding and loading are sometimes used to limit the spread and concentrate the magnetic field of the coil [10, 12].

2.6.1 Shielding and Loading

Shielding is used to reduce the interaction of the probes' magnetic field with irrelevant features in the vicinity of the probe. Shielding can be used to reduce effects such as transitions. Two types of shielding are typically used: Eddy current shielding or magnetic shielding. In magnetically shielded probes, a ferrite ring with high permeability and low conductivity is used to surround the coil. The ferrite creates an area of low magnetic reluctance and the probe's magnetic field is concentrated in this tighter area rather than spreading.

On the other hand, eddy current shielding uses a highly conductive nonmagnetic ring to surround the coil [10]. The coil's magnetic field that cuts the shielding generates eddy currents in the shielding ring and not in the irrelevant features outside the shielded region. Shielding is more effective at higher frequencies.

In some situations, the coils are wound around a ferrite core (ferromagnetic substance). Therefore the flux generated by the coil passes through the ferrite rather than air. Therefore, the ferrite core concentrates the field near the probe center. Probes with ferrite cores are more sensitive than air core probes and less affected by probe wobble and liftoff [10].

2.7 Eddy Current Inspection Process

The basic steps involved in an inspection with a surface probe are the following

1. Select and setup the instrument and probe.

2. Select a frequency to produce the desired depth of penetration.

3. Adjust the instrument to obtain an easily recognizable defect response using a calibration standard.

4. Place the probe on the surface and null the instrument.

5. The probe must be scanned over the surface in a pattern that will provide complete coverage of the area being inspected. Probe-to-surface orientation must be maintained as probe wobble can affect defect signal interpretation. In many applications, fixtures to help maintain orientation or automated scanners are used.

6. Monitor the signal for a change in impedance that might occur as the probe moves over a defect.

2.8 Eddy Current Testing in Steam Generator Inspection

In nuclear power plants, eddy current data obtained from steam generator tubes is collected by multi-frequency probes [13] as discussed in chapter 1. Three types of multi-frequency probes are commonly used: Bobbin probe, Rotating probe and Array probe.

26

2.8.1 Bobbin Probes

The bobbin probe is widely used in the nuclear industry for steam generator inspection. An air core probe oriented co-axially is called a bobbin coil. The probe provides for fast detection of degradation present in steam generator tubes. However, it's limitations include lowered detection capability in some regions of the steam generator tubes and poorer defect characterization abilities compared to advanced designs such as rotating probes. Therefore the bobbin probe is typically used for initial screening of the tubes followed by inspection using high-resolution probes. Bobbin coils can be divided into two classes - absolute and differential coils. Both absolute and differential coils have two bobbin coils placed adjacent to each other as shown in Figure 2.3. The absolute coil has a reference coil whereas in the differential coil, the difference signal is considered. The disadvantage of the absolute coil is that the defect is typically superimposed over a large signal (such as lift-off). Probe wobble and lift-off can also mask defects. The difference signal in a differential configuration is obtained by subtracting the induced voltage in one coil from the voltage of the other coil. Thus the effect of probe wobble and liftoff can be eliminated and the defect signal is enhanced. This differencing mechanism provides robustness to the system by reducing the effects of parameters like temperature
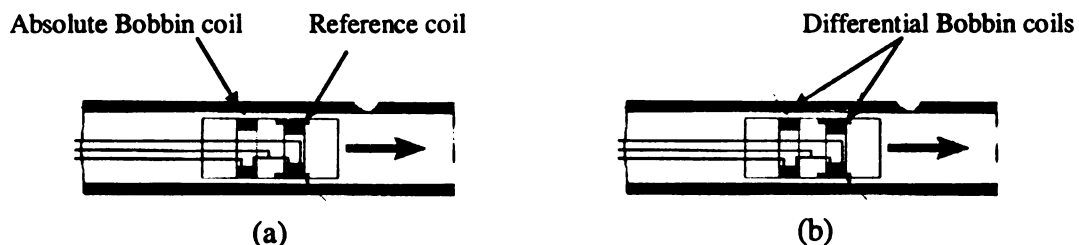
Figure 2.3 Bobbin probe (a) absolute configuration (b) differential configuration

and probe wobble. The sensitivity of the bobbin probe is very high to pitting, fretting wear and corrosion [14].

2.8.2 Rotating Probes

The rotating probe is shown in Figure 2.4. The probe consists of upto 3 coils rotating inside a tube at high speeds [15]. The coils are spaced $120°$ apart and each coil scans the inner surface of the tube in a helical path [16]. Rotating probes provide very high resolution compared to the bobbin probes. Also, the rotating probe collects several data points at each circumferential location in the tube whereas the bobbin collects one data point at each circumferential location. The rotation rate of the coils, pull rate inside the tube and coil diameter can be controlled and the tube can be inspected with high resolution.

One design commonly used for the rotating probe consists of two pancake coils and one plus point coil [16]. The plus point coil has a differential configuration leading to better signal to noise ratio in the presence of geometry changes and support structures in steam generators.
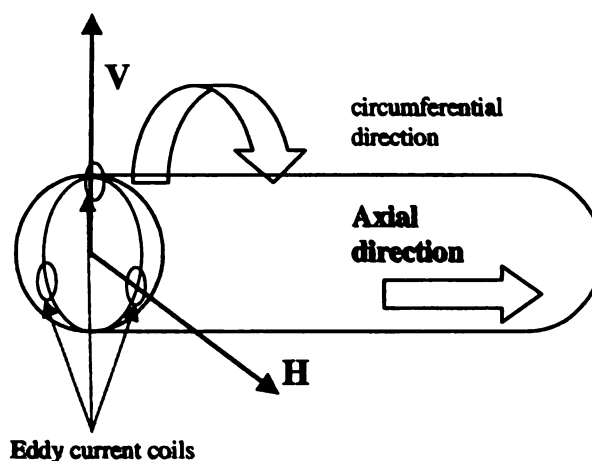
Figure 2.4 Rotating probe

28

2.8.3 Array Probes

The array probe is a relatively new probe used for inspecting steam generator tubes. The array probe has an array of pancake coils, and is designed to inspect steam generator tubes at speeds approaching inspection using bobbin probes with an accuracy similar to that of rotating probes [17]. Pairs of coils in this array are coupled in a transmit-receive fashion with laterally spaced transmit and receive coils.

The transmit coils are excited by alternating current at multiple frequencies. The transmit coils are active whereas the receive coils are passive. Current in the transmit coil generates an eddy current in the test material, and discontinuities in the test object disrupt the eddy current flow. The receive coils generate a voltage equal to the time rate of change of magnetic flux through the coil windings [18]. This voltage is interpreted as variations of phase and amplitude in the voltage plane.

As shown in Figure 2.6, flaws in the nearby test material that affect the eddy current flow and the magnetic flux through the receiver coil windings are detected and characterized by monitoring variations in the receive coil voltage.

Transmit-receive probes with laterally spaced pancake coils are directionally sensitive to the orientation of cracks. A set of coils is used to detect either circumferential

Input current

Induced currents

Transmit coil

Receive coil

Defect
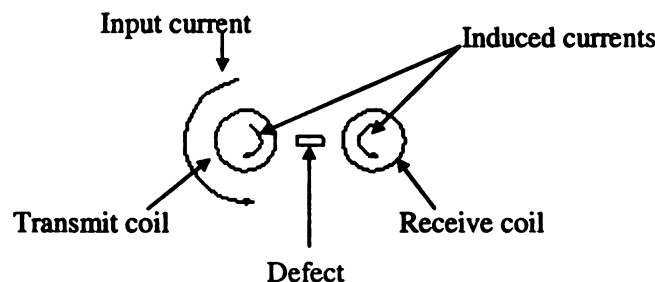
Figure 2.5 Transmit – receive configuration (adapted from [18])

29
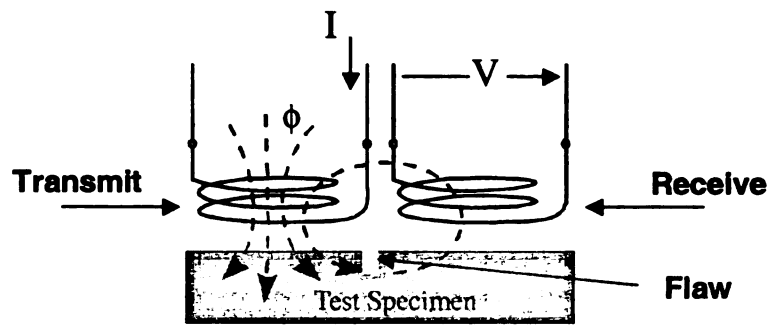
Figure 2.6 Transmit receive method (adapted from [18])
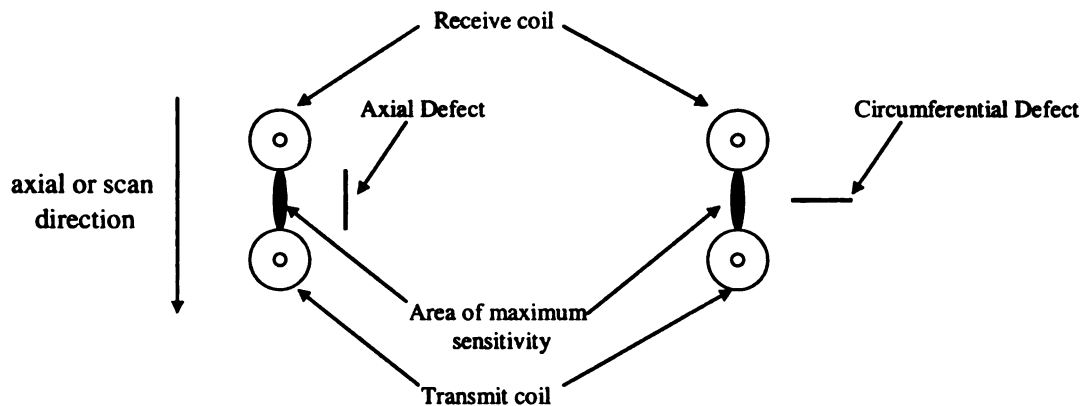
Figure 2.7 Sensitivity of coils

or axial flaws. Figure 2.7 explains the directional sensitivity of the transmit-receive pair. Both axial and circumferential coil sets detect the flaws that have no directional preference like volumetric defects.

The array probe consists of multiple transmit-receive coil pairs. Figure 2.8 shows a typical coil arrangement in a 16x3 coil probe. The coil pairs are arranged around the circumference of the probe in the form of a bracelet. The number of transmit-receive pairs on a typical array probe varies with the inner diameter of the tube. Since the probe does not rotate, the coils are in the same relative location with respect to the tube.
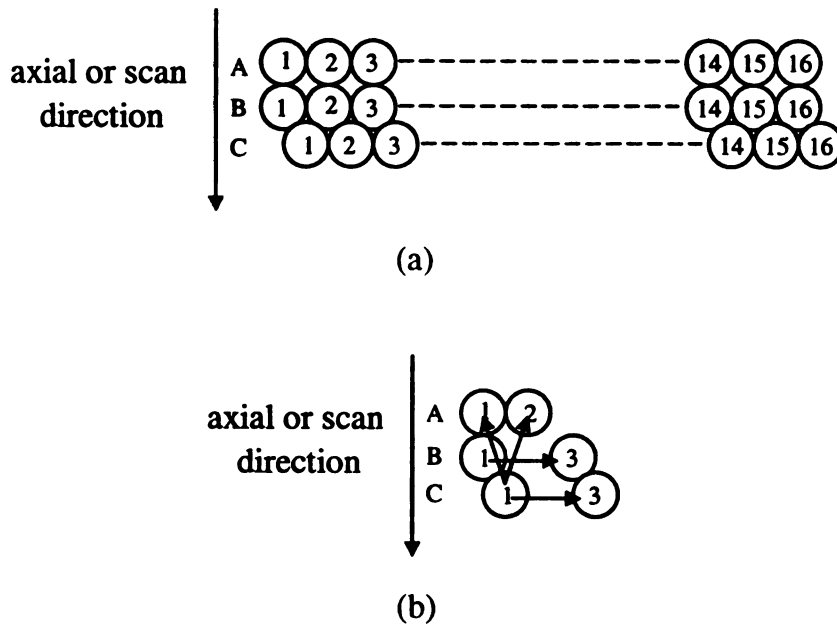
Figure 2.8 (16*3) 48-coil array probe (a) arrangement around the probe circumference (b) axial and circumferential channel formation

Figure 2.8(a) shows the 48 coils around the circumference of a tube in 3 rings. The generation of the first two axial and circumferential channels is shown in Figure 2.8(b). First, the two axial channels are obtained by transmitting from coil C1 to coils A1 and A2. Similarly the first two circumferential channels are obtained by transmitting from coil B1 to coil B3 and from coil C1 to coil C3. Other channels are formed in a similar fashion (by incrementing coil numbers by one). All coil pairs are multiplexed in time such that each receiver coil detects a signal from one transmit coil at any given time. For this probe design, a maximum of thirty two axial channels and two sets of sixteen circumferential channels may be generated. Each circumferential channel covers 22.5° and the axial channels cover 11.25° around the circumference of the tube. Data is collected as this probe traverses the tube with the coils in the same circumferential location relative to the tube. Figure 2.9 shows a typical array probe traversing a tube.

In general, after calibration, signals from probe motion and geometry changes remain horizontal and are essentially the same for both circumferential and axial channels. Increasing lift-off of the probe with respect to the sample shifts the signal to the left and decreasing lift-off to the right in the complex impedance plane. Tube expansions and dent signals are horizontal and do not interfere with the defect data and cracks produce vertical signal components in the complex plane [19, 20].
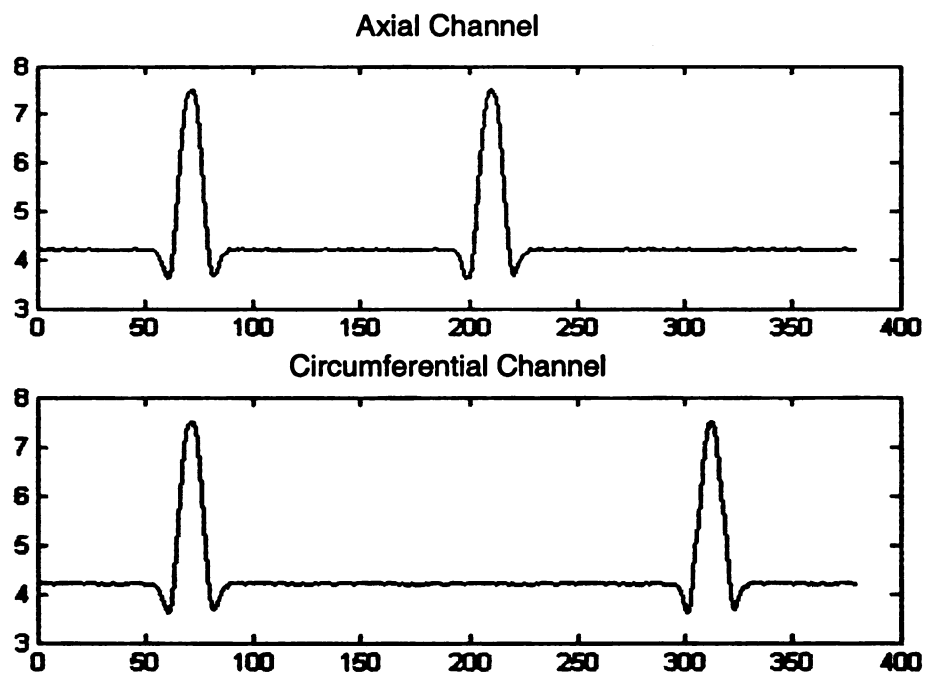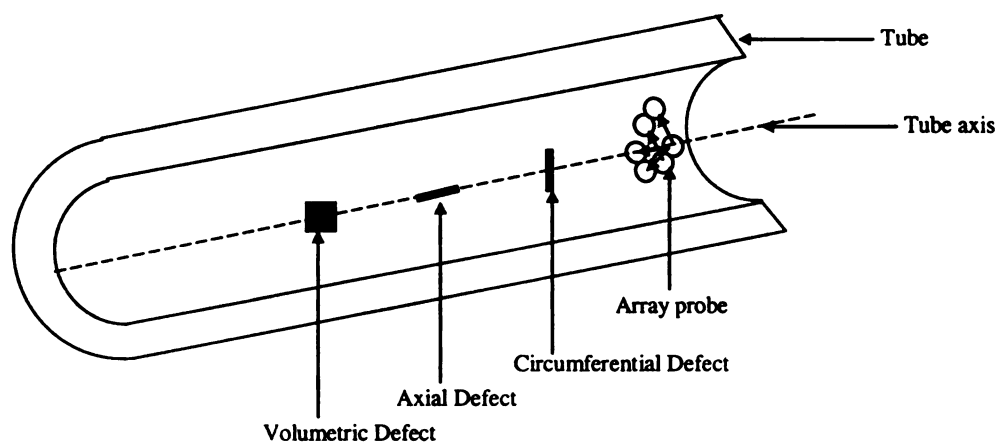
Figure 2.9: Response of array probe

CHAPTER 3. FINITE ELEMENT MODELING OF

TRANSMIT-RECEIVE COIL PAIR

Numerical models are used extensively in NDE for several reasons. Chief among these is the need to better understand the energy-material interaction, and the underlying physics of the inspection process. Commonly used numerical methods include the finite element method (FEM), finite-difference time-domain (FDTD), boundary element method (BEM), etc. These models can be used to develop a better understanding of the inspection process, especially in cases where the experimentation is not possible (or not easy). The use of models can be extended to design-for-inspection, where a product or structure is specially designed to allow for easy inspection during its lifetime.

A theoretical model provides information about the physics of the interaction between the input energy and the test material. Many times this interaction is complicated because of the presence of defects. The main purpose of a theoretical model is to determine the output when an experimental situation is impossible. Theoretical models also provide an inexpensive alternative to preparing defect samples, which can be time consuming. A good model can be used to determine the signal in circumstances where a
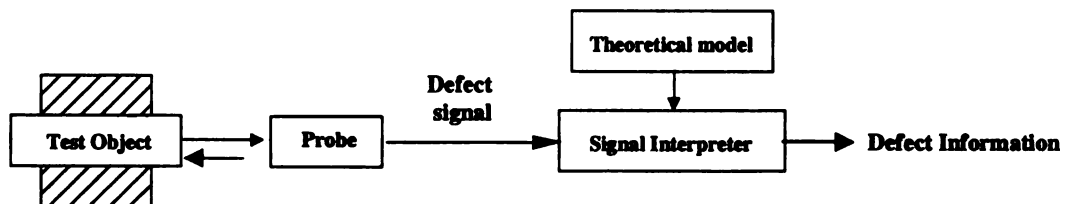
Figure 3.1 A general NDT system using a theoretical model (adapted from [5, 11])

real defect is expensive to manufacture in a controlled manner. With the advent of automated NDE systems in today's world, the need for training data for signal processing and calibration is ever growing [21]. The model can provide data for any test condition or parametric variation necessary. Parametric variations can be easily introduced into a model, while it can be a huge task to measure such variations in a sample. In many situations creating models is easier compared to preparing a sample. Models can also be used to generate reference signals for training a system [5, 11]. A mathematical model is necessary in order to be able to describe the interactions between the incident and induced currents, and identify suitable parameters for further signal processing like compensation, defect characterization in materials. Thus theoretical models play a vital role in NDT applications.

In electromagnetic NDE, the governing equations describing the energy-material interaction are Maxwell equations as discussed in Chapter 2. The solution has a closed form for simple problems or simplifying conditions. Finite element based numerical methods help in solving these problems in cases where the problem geometry is complex. The major issues associated with the FEM method are size of the problem and resources based on the size. The development of a three dimensional problem for finite element solution is relatively more tedious and time consuming when compared to a two dimensional problem. The computing resources needed are much more compared to two-dimensional analysis as the problem geometry, solution and visualization can be complex. A correct formulation of the field equations and the uniqueness of the solution is very important.

This section of the thesis describes the development of a two-dimensional FEM for studying the array probe inspection process. A 2D FEM is used to predict the output signal of a transmit-receive eddy current coil configuration for an axi-symmetric case.

In eddy current techniques, defect modeling is based on the fact that the volume of the defect is a local geometrical discontinuity and results in a change in the properties of the material [22]. The 2D model is based on a magnetic vector potential formulation of eddy current phenomena. This formulation is general and results in easy application of boundary conditions. The magnetic vector potential is obtained by continuing from Eq. (2.1) in Chapter 2 to get:

$$(\frac{1}{\mu})\nabla^2 \vec{A} = -\vec{J}_s + j\omega\sigma \vec{A} \qquad (3.1)$$

Solving Eq. (3.1) with appropriate boundary conditions (Dirichlet or Neumann conditions) gives the magnetic vector potential [5, 11]. For the two-dimensional case, Eq. (3.1) is simplified to

$$\frac{1}{\mu}(\frac{\partial^2 \vec{A}}{\partial x^2} + \frac{\partial^2 \vec{A}}{\partial y^2}) = -\vec{J}_s + j\omega\sigma \vec{A}. \qquad (3.2)$$

3.1 Two Dimensional Finite Element Formulation

As stated earlier, the 2D FEM uses a magnetic vector potential formulation. This formulation assumes:

- The source current density and the magnetic vector potential vary sinusoidally with time. Harmonics in both the source and induced fields are absent.

- Eddy currents in the source coils are neglected.

- Electrical conductivity and magnetic permeability of test materials are constant in each element in the solution region. Spatial variations in permeability can be modeled as long as they are constant within each element.

A general energy functional for electromagnetic field problems can be expressed as [11]

$$F = \int_V (S - I + D)dv.$$ (3.3)

where S is the stored energy because of the magnetic field, I is the input energy from the incident current densities and D is the dissipated energy from the eddy current densities in the conducting regions of the model excluding the sources.

The solution to the equations is obtained by finding a set of functions A which minimize the energy functional $F(A)$. It is not possible to minimize the function everywhere, so it is minimized at a set of discrete nodes in the solution domain. The discretization of the solution domain is very important since the number of elements and nodes and their location in the domain affects the solution. The process of discretizing is also termed as meshing. A very coarse mesh with few nodes introduces large errors while a fine mesh with too many nodes results in a longer time in the solution process and complicated. Efficient meshing techniques play an important role in the accuracy and efficiency of the model. A variety of basic elements can be used in the finite element model. Some of the commonly used elements are tetrahedrons, triangular prisms, and hexahedrons for three-dimensional models and triangles for two-dimensional models. A node can be defined at each vertex of the basic element. In higher order elements there can be nodes between two vertices or at the centroid of the element.

In this thesis, triangles are used as the basic elements. The solution domain is subdivided into finite elements with no restriction over the size and number of the

elements. The density of the elements depends on the geometry. Dense elements are used in locations with high curvatures. Material interfaces in the solution domain and on the boundaries coincide with element boundaries. An element does not have more than one material in the region. Each component of conductivity, current density, permeability and flux density is assumed to be constant in the element, and all quantities calculated are either values at nodes or associated with the elements such as energies. The magnetic vector potential is assumed to be zero at the boundaries of the solution domain by assuming these locations are far enough from the source.

The energy function in Eq. (3.3) is minimized at every node in the solution domain [5, 11], i.e.,

$$\frac{\partial F(\vec{A})}{\partial A_{ki}} = 0, \quad i = 1,2,3,\ldots\ldots,N \; ; \quad k = x, y \tag{3.4}$$

where N is the total nodes in the solution domain. Neumann boundary conditions (normal derivative of the function is known) or Dirichlet boundary conditions (the function A or ϕ are known at the boundary) can be applied. To save computing resources the boundaries can be close but can increase the error introduced in the solution. A tolerance limit has to be established on the magnitude of error and the closeness of boundaries. The solution is obtained by applying suitable solver algorithms (slice successive over-relaxation (SSOR), gradient methods etc.) to solve for A.

3.1.1 Induced Voltage Calculations

The magnetic vector potential is an auxiliary function and quantities such as the induced voltage, coil impedance, stored and dissipated energy, and eddy current density can be calculated from it [23]. Specifically, the induced voltage is calculated from $\vec{A}$ as

$$U_i = -j\omega \sum_{i=1}^{k} \Delta_i A_{ci} \, .$$

(3.5)

where Δ_i is the element cross sectional area and A_{ci} is the value of the magnetic vector potential in the element i of the finite element domain.

3.2 FEM of a Transmit-Receive Coil Pair

A two-dimensional axi-symmetric finite element model was developed to predict signals from a transmit-receive coil configuration. The two dimensional finite element model study provides significant insight into the eddy current signal from the receiver coil. The aim of the experiment is to investigate perturbations in the eddy current signal due to various testing parameters like the flaw depth, ID/OD effects, offset with respect to the flaw center, excitation frequency and liftoff.

The geometry studied is that of steam generator tubing in a nuclear power plant (Figure 3.2). Figure 3.2 shows a schematic of the model. Each steam generator consists of multiple Inconel 600 tubes (0.75" O.D. and 0.043" wall thickness). In this model, an absolute transmit-receive coil pair is modeled and the measured quantity is the induced voltage in the receiver coil. An important feature of the modeling of the transmit-receive eddy current coils is the movement of the probe relative to the flaw. The voltage is recorded at several discrete points as the probe moves across the flaw.

The parameters of the model are as follows: The coil material is assumed to be copper ($\mu_r = 1$ and $\sigma = 5.77 \times 10^7$ S/m). A 10mm long axial defect is introduced in an Inconel 600 tube at various depths (40%, 60%, 80% and through wall). Both I.D. and O.D. initiated cracking was studied by using the model.
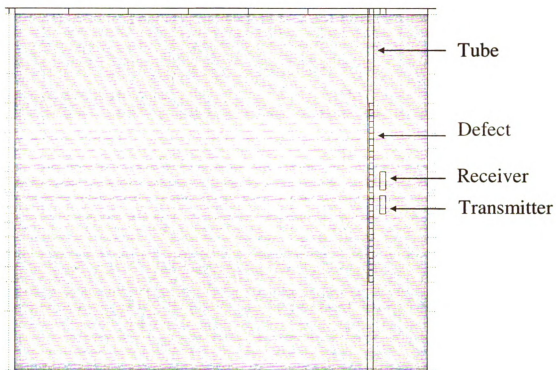
Figure 3.2 An Inconel 600 tube with transmit –receive coil pair
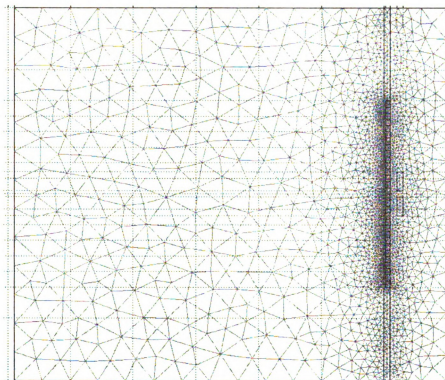
Figure 3.3 Mesh for the absolute transmit-receive coil pair in Inconel 600 tube

The tube material (Inconel 600) is assumed to have $\mu_r = 1$ and $\sigma = 1*10^6$ S/m [11]. The transmit and receive coils both have a diameter of 3 mm. The separation between the coils is 4 mm.

The dimensions of transmit and receiver coils are assumed to be identical. The transmit coil is excited with a constant current density of 10^3 A/m^2 at various frequencies (100 kHz, 200 kHz, 300 kHz and 400 kHz). The receive coil is passive and the complex induced voltage in the receive coil is obtained from $\vec{A}$. This procedure is repeated for the various positions of the probe for a complete trajectory across the defect. The same procedure is repeated by changing various parameters such as frequency, depth, ID/OD and liftoff, etc.

The following studies were conducted using the finite element model:

1. Prediction of the receive coil response signal for a complete trajectory across the defect.

2. Prediction of eddy current signal trajectories at different frequencies for I.D./O.D. defects

3. Prediction of eddy current signal for varying flaw depths

4. Prediction of eddy current signal for changing lift-offs

The results of these simulations are presented in Chapter 5.

3.3 Compensation Algorithms

Compensation algorithms are developed based on the data collected from the FEM model. The basic idea is to compensate for various experimental parameters that affect the measurement from the receiver in the transmit-receive probe. Compensation algorithms can be developed to compensate for various factors like probe velocity, origin

of sampling, permeability [24] and lift-off. This thesis deals specifically with lift-off compensation. Mandayam [24] presents various invariant techniques and transformations for compensation. An invariant represents a quantity which is definite to an object. It must be invariant under any choice of co-ordinate system. As an example of a transformation, consider a co-ordinate system XY in Cartesian co-ordinates. Let $p(x, y)$ be a point in this co-ordinate system. Consider another co-ordinate system X'Y' which is translated by a factor (x_a, y_a) and rotated by an angle θ. The transformation of p into X'Y' is given by

$$x' = x\cos\theta - y\sin\theta + x_a \tag{3.6}$$

$$y' = x\sin\theta + y\cos\theta + y_a. \tag{3.7}$$

Eqs. (3.6) and (3.7) describe the property of a point in another co-ordinate axis. In general they represent a characteristic of an object in another domain. The Euclidian distance between the two points remains unchanged irrespective of the co-ordinate axes [24]. This distance remains unchanged irrespective of the co-ordinate axes. A similar idea is applied to develop compensation algorithms to compensate for lift-off in array probe eddy current data [25]. This study investigates the use of affine transformations, as well as neural networks, for achieving lift-off compensation. In addition, the use of multifrequency measurements for compensation is also investigated.

3.3.1 Affine Transformation Based Methods

An affine transformation is a transformation that preserves collinearity and ratios of distances [26]. Expansion, dilation, rotation and translation are some examples of affine transformations. In this approach, an affine transformation is used to compensate for lift-off. This approach tries to compensate for liftoff by utilizing signals at different

lift-offs and mapping them to a signal at minimum lift-off at a particular frequency. The optimal transformation is determined through the use of a training data set. This problem can be viewed as an optimization problem. A non-linear curve fitting approach [27] is used to determine the transformation parameters. This approach finds the transformation coefficients that best-fit the data at multiple lift-offs for various depths to the corresponding signals at minimum liftoff for one particular frequency. The transformation is expressed as

$$Y = AX .$$ (3.8)

where

$$A = \begin{pmatrix} a_{1,1} & a_{1,2} \cdots\cdots\cdots\cdots a_{1,m} \\ a_{2,1} & a_{2,2} \cdots\cdots\cdots\cdots a_{2,m} \\ \vdots & \ddots & \vdots \\ \vdots & & \ddots & \vdots \\ a_{m,1} & a_{m,2} & \cdots & \cdots & a_{m,m} \end{pmatrix}$$ (3.9)

is the optimized transformation matrix, and the columns of X contain the signals at multiple lift-offs. The matrix Y contains the target signals. The nonlinear curve fitting technique solves the problem in the least squares sense, i.e., given the input data X, and the observed output Y, coefficients a are found such that they best fit Eq. (3.10).

$$\min_{a} \frac{1}{2} \|F(a, X) - Y\|^2 = \frac{1}{2} \sum_{i} (F(a, X_i) - Y_i)^2$$ (3.10)

Consider a function f(x) at m values

$$y_1 = f(x_1), \ldots, y_m = f(x_m)$$ (3.11)

Let the function be dependant on n parameters $f(x; a_1, \ldots, a_n)$, and m such equations are obtained for m values of x. These equations can be solved to obtain $a_1, \ldots, a_n$, which best satisfy the m equations. Consider an initial value for a_i and define

42

$$db_i = y_i - f(x_i; a_1, \ldots\ldots a_n). \tag{3.12}$$

Now an estimate for changes da_i to reduce db_i to 0 is given by

$$db_i = \sum_{j=1}^{n} \frac{\partial f}{\partial a_j} da_j \bigg|_{xi,a} \tag{3.13}$$

for i=1,.....,n, where a=(a_1,......a_n). This can be written in component form as

$$db_i = A_{ij} da_i \tag{3.14}$$

or matrix form as,

$$db = Ada \tag{3.15}$$

where A is an m x n matrix.

Applying A^T to both sides gives

$$A^T db = (A^T A)da. \tag{3.16}$$

Defining

$$P \equiv A^T A \tag{3.17}$$

$$Q \equiv A^T db, \tag{3.18}$$

the following matrix equation is obtained

$$Pda = Q \tag{3.19}$$

which can be solved for da using techniques such as Gaussian elimination [28, 29]. This is then applied to a and a new db is calculated. This procedure is applied iteratively until da is smaller than a specified limit.

3.3.2 Artificial Neural Networks

Artificial Neural Networks (ANN) are models based on the structure of the brain. The power of natural neural networks comes from the complexity of the vast number of

basic components called neurons and the multiple connections between them. The brain has the ability to learn through experience and a neural network mimics the brain's learning capability. Neurons and their interconnections (synapses) are the important elements for information processing in a biological network. Most neurons possess tree like structures called dendrites, which receive incoming signals from other neurons. Signals are transmitted as electrical pulses through axons that carry the output of a neuron to other neurons. Each neuron is connected with thousands of other neurons and it collects signals at its synapses by adding all the excitatory and inhibitory influences acting on it. The effect of each input is multiplied by a weight to denote the strength of the synapse. The weighted signals are then added to produce an output response. The system derives information by learning from the different inputs it receives and trains itself using its complex structure. This is similar to the learning process in ANN.

ANN are used in a variety of applications from function approximation to pattern recognition and signal processing. ANNs are a form of a multiprocessor computer system with simple processing elements, high degree of interconnection and adaptive interaction between elements. They are highly connected systems with variable weights at nodes interconnecting the nodes [30]. The network acquires knowledge through a learning algorithm which changes the weights to achieve a particular goal [31]. Supervised learning networks such as multi-layer perceptrons (MLP) represent one stream of development in neural network theory. Two stages are involved in the supervised learning network. The networks learn by adaptively updating the synaptic weights of the interconnections. The weights are updated based on the information obtained from training samples. The network trains itself to match the desired output as input patterns

are presented to it. After training, the network is tested with patterns not present in the training database, and it gives a generalized output based on the training. The other major category of neural networks are unsupervised neural networks. In this case the training set consists of input training patterns only. The networks learn to adapt based on the experience of the previous input training patterns. In the following sections, two common types of neural networks, multilayer perceptrons and radial basis function networks (RBF) are discussed.

3.3.2.1 Multilayer Perceptron (MLP)

The Multilayer perceptrons (MLP) are of the most widely used networks. The MLP is an extension to the simple perceptron, which can distinguish classes that are linearly separable [32].

In multilayer perceptrons, the inputs are processed through successive layers of neurons. The input layer has a number of neurons equal to the number of variables in the problem. The output layer, where the response is available, has a number of neurons equal to the desired number of quantities computed from the inputs. The one or more layers in between are called hidden layers. All the nodes in all the layers are fully connected to each other and each connection has its own weights. Inputs propagate through the network in the forward direction from input layer to hidden layers to the output layer. The model of each neuron in the hidden layers consists of a non-linearity. A typical non-linearity is the logistic function

$$y_j = \frac{1}{1 + e^{-x_j}}.$$ (3.20)

where y_j is the output and x_j is the net activity level of neuron j.
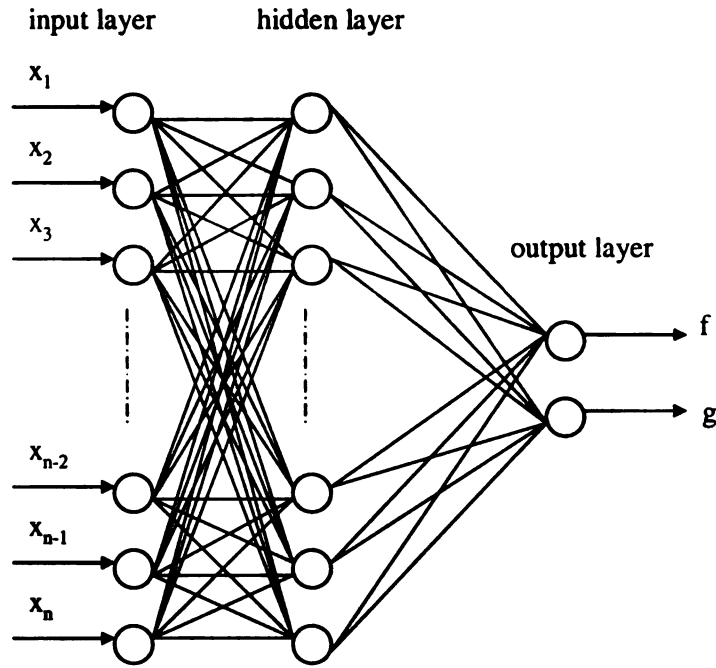
Figure 3.4 Multilayer perceptron

A typical MLP is shown in Figure 3.4. The back propagation algorithm [31, 32] is used commonly for learning with supervision from training samples from known classes. This algorithm consists of a forward and a backward pass. In the forward pass, an input is applied to the network, propagated through the network, and an output is generated as the response of the network. During the backward pass, the error signal, which is the difference between the desired signal and the actual response of the network, is propagated backward through the network for updating the weights of the MLP [33]. The weights are updated to make the actual output converge to the desired output.

Given an input vector x_{ip} and desired output d_{kp} where i=1,2,...N are the input nodes, p is the number of input patterns in the training data, and k =1,2,...M is the node index in the output layer, the total input at node j in the hidden layer is

$$n_{jp} = \sum_{i=0}^{N} w_{ji} x_{ip}$$ (3.21)

where j=1,2,...L is the node index of the hidden layer.

The corresponding output of the node is

$$z_{jp} = \frac{1}{1 + e^{-n_{jp}}}$$ (3.22)

and the output of the node k at the output layer is

$$y_{kp} = \sum_{j=0}^{L} z_{jp} w_{kp}$$ (3.23)

A measure of error due to pattern x_p is given by

$$E_p = \frac{1}{2} \sum_{k=1}^{M} (d_{kp} - y_{kp})^2$$ (3.24)

where $e_{kp} = d_{kp} - y_{kp}$ is the error at an output node k. To find weights w_{ji}, w_{kj} that

minimize the error, a gradient based error minimization procedure [32] is used. The

weights in the network are adjusted as

$$w_{kj} \leftarrow w_{kj} - \eta \frac{\partial E_p}{\partial w_{kj}}$$ (3.25)

$$w_{ji} \leftarrow w_{ji} - \eta \frac{\partial E_p}{\partial w_{ji}}$$ (3.26)

where $\eta > 0$ is a learning rate. Using the above equations and the chain rule [32]

$$\frac{\partial E_p}{\partial w_{kj}} = -e_{kp} z_{jp},$$ (3.27)

the weight update rule for the output layer can be derived as

$$w_{kj} \leftarrow w_{kj} + \eta e_{kp} z_{jp}$$ (3.28)

Similarly the weight update rule for the hidden layer can be derived as

$$w_{ji} \leftarrow w_{ji} + \eta e_{jp} x_{ip}$$
(3.29)

This algorithm is called the backpropagation algorithm.

3.3.2.2 Radial Basis Function Networks

Radial basis function (RBF) networks are another commonly used class of networks. RBF networks are a special case of MLPs, where the neuron activation functions are radially symmetric [33]. Commonly used basis functions include Gaussians and Laplacian functions. The RBF neurons describe patterns better than perceptrons when the classes can be described using radially symmetric basis functions. A general form of a radial basis function is

$$h(x) = \phi((x-c)^T R^{-1} (x-c)).$$
(3.30)

where ϕ is the radially symmetric basis function, c is the centre of the basis function and R is some metric.

Figure 3.5 shows an RBF network with inputs $x_1, x_2, \ldots \ldots x_n$ and outputs $y_1, \ldots y_m$. The RBF has one hidden layer of basis functions or neurons. At the inputs, the distance between the input vector and the neuron center [34] (center represented by the basis function) is calculated as

$$d = (x-c)^T R^{-1} (x-c).$$
(3.31)

The output is then obtained by applying the basis function to this distance. The centers are chosen using the k-means clustering algorithm [35], and the output is formed by a weighted sum of the neuron outputs as in Eq. (3.32):

$$f(x) = \sum_{j=1}^{m} w_j h_j(x)$$
(3.32)

48
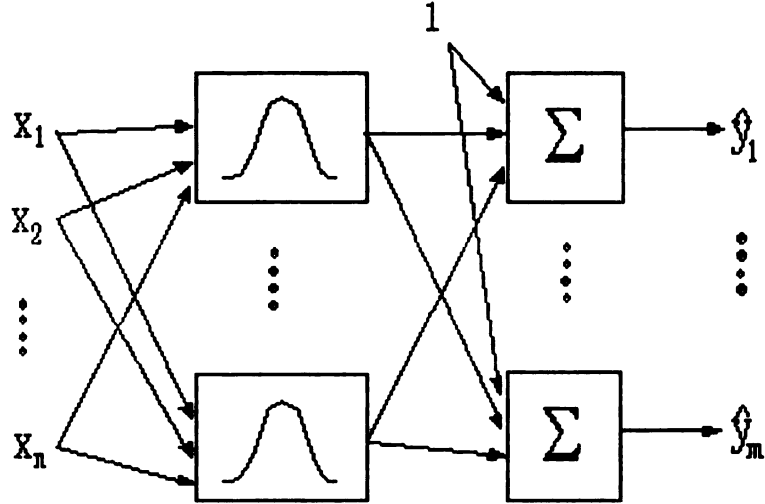
Figure 3.5 Radial basis function network

where w_i is the weight of each element. Thus, the network performs a non-linear transformation by forming a linear combination of the basis functions. A Gaussian basis function is shown in Figure 3.5. Once the network structure is specified, it can be trained using a set of data containing N input and output pattern pairs. The parameters of the basis functions representing the centers are computed first. A good algorithm for training is one that minimizes the mean square error. The training algorithms for RBFs are iterative and start with an initial parameter set and iteratively decrease the mean square error by updating the network parameters. The main advantage of RBF is over MLP is that its convergence time is very fast.

3.4 Compensation Algorithm Details

The simulated data obtained from the FEM is used to compensate for liftoff. All three algorithms, namely, affine transformation, MLP and RBF networks, are used. The process consists of two stages – training and testing. In both training and test cases, data at higher liftoffs are transformed to a minimum liftoff case (0.5mm). signals with liftoffs

49

at 1, 2 and 3 mm are used for training and signals with liftoffs at 1.5 and 2.5 mm are used for test. The training process uses the training data and computes the parameters of the appropriate algorithm (affine transformation, MLP neural network or RBF neural network). The parameters are then applied to the test data to demonstrate the performance of the algorithm. The compensation is performed for single and two frequencies. In the single frequency case, data at higher liftoffs at one frequency from flaws at different depths are used to develop a compensation algorithm that transforms these signals to a minimum liftoff signal at the same frequency. In the two frequency case, data at higher liftoffs at two frequencies for several depths are used to develop a compensation algorithm that transforms these signals to a minimum liftoff signal at one of the two frequencies. Simulated data from the FEM model was used in all cases. Each signal consists of 24 samples of the eddy current measurement as the probe moves across the flaw. Several signals, corresponding to multiple flaw depths and inspection frequencies, were generated using the FEM model, and used in the development of the compensation algorithms. The affine transformation used a matrix with 48x48 unknowns that were determined using the transformation data. Similarly, the neural networks, each used a single hidden layer and had 48 nodes in both the input and output data. The input, in all cases, consisted of the real and imaginary components of the eddy current measurement, concatenated together. Results of the compensation algorithms are presented in Chapter 5.

CHAPTER 4. ANALYSIS OF ARRAY PROBE EDDY CURRENT DATA

This chapter starts with an overview of requirements for signal processing of array probe eddy current data collected from steam generators in nuclear power plants. Algorithms for detection and classification of degradations versus non-degradations are then presented. The major issues in signal processing of array probe data are noise reduction and data decomposition. The analysis demands several preprocessing steps, which influence the overall detection performance.

Degradations in steams generators in nuclear power reactors are a key issue in the nuclear power industry. Typically, analysis of eddy current data is done manually. However, the move to higher resolution probes (such as rotating probes and array probes) has resulted in large amounts of data, with faster analysis requirements. Hence, there is a need to automate the analysis procedure to detect degradations. Typically, the location of degradation needs to be determined, with degradation depth determination also necessary in some cases. Most of the degradations are localized, in the sense that their size is very small compared to the tube length. The discrimination between defects and non-defects is based on the waveform characteristics of individual signals obtained from the array probe and parameters derived from these waveforms.

Data collected using array probes requires more storage space when compared to other eddy current probes such as bobbin or rotating coil probes. Data collected from a full-length scan of a typical 70' long steam generator tube with a 14x2 coil array probe requires around 20 MB of storage space. In general, the larger the number of coils in the

array, the larger the number of data channels and the larger the amount of storage required. The total number of channels of data collected using an array probe is calculated as

$$Ch = (A + C) * F .$$
(4.1)

where

A=number of axial channels in array probe

C=circumferential channels in array probe

F=number of frequencies at which data is collected

The one-dimensional data obtained from each coil is converted to a 2D image representing the tube as shown in Figure 4.1. The axial or circumferential channels collected at each frequency are arranged next to each other as they are obtained from the array probe to form an image representing a tube that has been cut open along the axial direction. Figure 4.1 shows an example of 16 circumferential channels arranged along the circumferential direction to form an image. The vertical axis represents the axis of the tube. These images are then processed further to analyze the data. The analysis is performed in three distinct stages: preprocessing, detection and classification. Preprocessing extracts important information from the data, which is used in further analysis of the data. The detection stages are necessary to identify potential flawed indications in the tube and classifiers assign these indications into defect and non-defect classes, as well as determine the type of defect (axially or circumferentially oriented, etc.). The preprocessing is implemented in several steps as shown in Figure 4.2. A discussion on the function and necessity of each preprocessing step follows.

Field data (100 KHz) vertical

Axial direction

Circumferential direction

Figure 4.1: 2D image of the 16 circumferential 1D channels

Raw Data

Interpolation

Calibration

Data Segmentation

Support Suppression

Filtering

Baseline Alignment and Median Suppression

Multifrequency Mixing

Median Filter

Bandpass Filter

Continuous Wavelet Transform
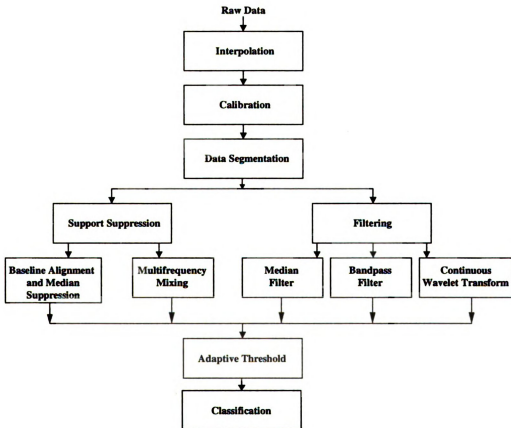
Adaptive Threshold

Classification

Figure 4.2: Preprocessing

4.1 Interpolation

In the array probes considered in this study, the total number of axial channels at each frequency are double the number of circumferential channels at the same frequency. This gives rise to a difference of resolution in the axial and circumferential channels along the circumferential direction. For instance, a 16x2 coil array probe generates 32 axial channels and 16 circumferential coils per frequency. These numbers are based on the design of the array probe discussed in Figure 2.8 of chapter 2. In order to eliminate this difference in resolution between axial and circumferential channels, a linear interpolation method is used for circumferential channels. An additional channel is introduced between two adjacent channels in circumferential coils by means of linear interpolation. If x_i and x_{i+1} are two consecutive circumferential channels, the interpolated channel is given by

$$x_{int} = \left(\frac{x_i + x_{i+1}}{2} \right).$$

(4.2)

The process is similar for real and imaginary components of the eddy current signal. This is performed for all circumferential channels at all frequencies in the array probe data.

4.2 Data Segmentation

Data from different parts of the tubes have distinct characteristics. For example, signals from tube sheet and tube support plate regions can be relatively noisy compared to free span regions. Dividing the data carefully into appropriate segments can provide significant analytic benefits. Different locations of the tubes can be visualized individually facilitating data analysis by including or neglecting certain portions of the

tube. Segmenting a tube also brings about flexibility in analyzing the data. Once the segmentation is completed, the user can process segments (or suppress them) according to one or more criteria. For instance, lift-off variations in the U-bend region of some tubes can cause signal level changes between different channels. Figure 4.3 shows a typical section of a U-bend region in a steam generator tube, with the intrados and extrados regions in the tube. In this situation the intrados and extrados regions might demand separate algorithms. Thus data segmentation is a necessary aspect of any algorithm developed for different regions in the tube.

Segmentation helps to split the data into regions highlighting or detecting the discontinuities between multiple objects (freespan, structures) in the data. Typical segmentation methods segment eddy current images based on the presence of edges or discontinuities [36]. These techniques make use of derivatives to identify edges in images i.e., the position of an edge is given by a maxima or minima in the first order derivative or a zero crossing in the second-order derivative. Different types of edge detection algorithms include gradient based methods, regularized edge detection and edge detection using zero crossings [36]. Given a signal g(x), the first order derivative is given by

$$\nabla g(x) = \frac{\partial g}{\partial x}. \tag{4.3}$$

and the magnitude of this gradient is given by

$$|\nabla g(x)| = \left|\frac{\partial g}{\partial x}\right|. \tag{4.4}$$

The second order derivative (Laplacian) is calculated as

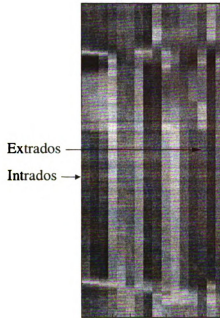$$\Delta = \frac{\partial^2 g}{\partial x^2}. \tag{4.5}$$

55

Figure 4.3 A typical U-bend region showing intrados and extrados

The gradient and Laplacian are invariant upon rotation [36]. When the Laplacian operator is applied to signals, the low frequency or slowly varying components are weakened and high frequency components are enhanced or stay intact. All structures (edges) present in signals are high frequency components, and therefore can be easily detected using edge detection methods.

4.3 Signal Suppression

The elimination or reduction of an unwanted signal is called signal suppression. In eddy current analysis, it is desirable to suppress signals from external support structures so as to enhance signal to noise ratio and consequently, enhance flaw detection. Data segmentation and automatic support detection makes it possible to selectively suppress and process the signals from structures present in steam generators. The support suppression methods studied here are median subtraction and multifrequency mixing.

4.3.1 Baseline Alignment and Median Suppression

Median subtraction basically subtracts the median value in each channel (along the axis of the tube) to remove the DC component present in the data, thereby aligning the baseline in each channel. Subsequently the median value at each axial location across channels is subtracted, suppressing the signal from supports in the tube. Let x_c be the signal from one axial or circumferential channel. Then, the DC component in the vector x_c is removed by subtracting the median m_c of the channel

$$m_c = median(x_c) \tag{4.6}$$

$$x_{new} = x_c - m_c \tag{4.7}$$

Let m_a be the median value of a signal x across all channels at a particular axial location. Then, the operation

$$x_s = x - m_a \tag{4.8}$$

suppresses support signals. This process is applied to the support regions in the data.

4.3.2 Multifrequency Mixing

Mixing is a commonly used method to suppress tube support plates [8]. As in the case of compensation discussed in Chapter 3, mixing uses an affine transformation to transform signals at one (low) frequency to another, higher frequency. The transformed signal is then subtracted from a signal at the higher frequency to remove support signals.

The approach finds the transformation coefficients that best-fit the data at one frequency to the data at another frequency. The transformation is expressed as

$$R = A * Y \tag{4.9}$$

where

$$A = \begin{pmatrix} a_{11} & a_{12} \\ a_{21} & a_{22} \end{pmatrix} \tag{4.10}$$

is the transformation matrix, Y is the low frequency signal and R is the desired higher frequency signal. Typically, Y and R are signals at two different frequencies, and are obtained by inspecting a simulated support plate on the calibration standard. The parameters of the affine transformation, once determined using these signals, are applied to other data to suppress supports. Specifically, let Y_1 and R_1 be two signals (at two frequencies). Then, the support suppressed signal X_s is suppressed as

$$X_s = R_1 - A * Y_1. \tag{4.11}$$

A non-linear curve fitting approach for mixing (discussed in Chapter 3) is used to determine the parameters of the affine transformation. The nonlinear curve fitting technique solves the problem in the least squares sense as given by Eq. (3.10).

4.4 Filtering and Denoising

Any undesirable signal other than defect signals present in the steam generator eddy current array probe data is considered noise. Sources of noise include signals from liftoff, U-bend effects, structures etc., and large levels of noise reduce the ability to detect defects. Several approaches are investigated in this study for noise reduction, including median filtering, band-pass filtering and the continuous wavelet transform (CWT). These are described in the following sections.

4.4.1 Modified Median Filters

Median filtering is an approach used to eliminate low frequency noise present in the data. In other words, it acts as a high pass filter. Median filters belong to the class of edge preserving smoothing filters, which are non-linear filters for signal enhancement
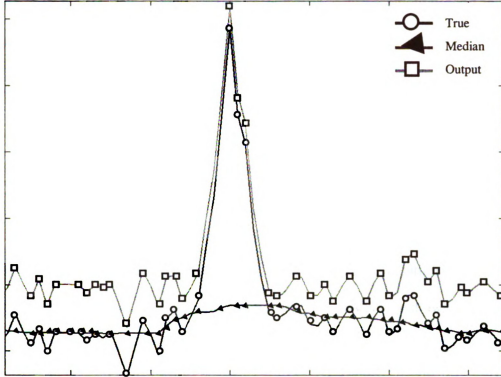
Figure 4.4 Modified median filter

[37]. These filters smooth the data while keeping small and sharp details. Median filtering is a simple and very effective noise removal filtering process [36, 37, 38]. Figure 4.4 shows an example of modified median filtering. A median signal is computed from the original signal as shown in the figure. This median signal is subtracted from the original signal to obtain the filtered data. The filtered data does not contain low frequency components and high frequency defect information is retained. The median signal is obtained by computing median values within a sliding window of length w. Let $x(i)$ be the original signal and y be the median signal given by

$$y(i) = median\{x[j], j \in w_i\} . \qquad (4.12)$$

Each point in y, $y(i)$, is the median value of points in x in the neighborhood w_i around sample i. The size of w is data-specific. The high frequency components and defect signals are enhanced by subtracting the median signal $y(i)$ from the original as

$$f(i) = x(i) - y(i).$$ (4.13)

where $f(i)$ is the median filtered signal.

4.4.2 Band Pass Filter

This type of a filter transmits a band of frequencies and rejects frequencies outside this band. The width of the pass band depends on the application at hand, and the transition from pass-band to stop-band can be sharp or gradual as shown in Figure 4.5. Filters with multiple pass-bands can also be designed to meet specific application needs. In eddy current analysis, band pass filters are useful in suppressing signals from transitions, periodic noise as well as high frequency noise. However, defect signals and noise should be in different frequency bands in order for such a filter to work. The band pass filter can also be used to remove the effects of intrados and extrados variations present in U-bends.

An ideal bandpass filter passes some range of frequencies without distortion and suppresses all other frequencies. It has a rectangular magnitude response given by

$$H(\omega) = \begin{cases} 1 & f_1 < \omega < f_2 \\ 0 & elsewhere \end{cases}.$$ (4.14)

However, such a filter is not physically realizable because its time-domain representation is non-causal and it is not stable. Practical bandpass filters approximate the ideal filter and deciding on the best approximation involves a compromise between various properties of the filter such as filter order, attenuation rate, cutoff frequency,
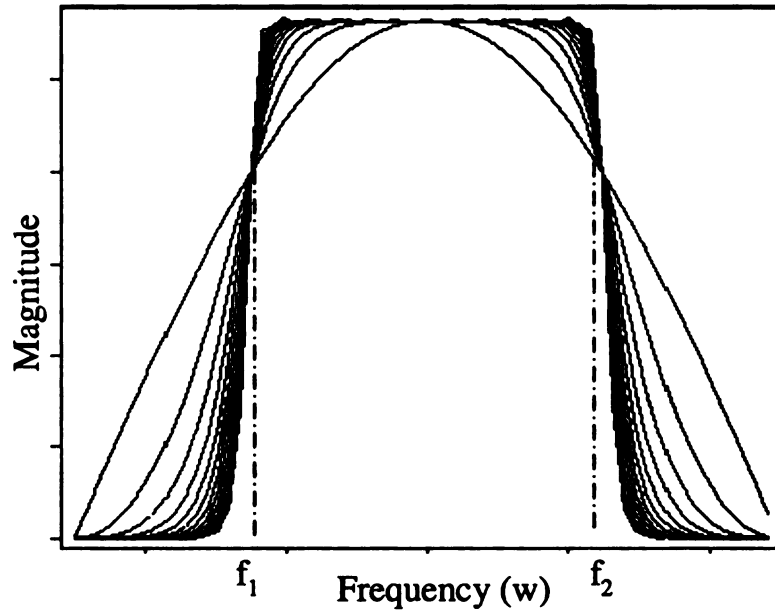
Figure 4.5 Bandpass filter

transient response and pass/stop band ripple. While several approaches to filter design are

known (IIR filter design using Butterworth, Chebyshev, Bessel or Elliptic [39]

prototypes, or FIR filter design using windowing or the Remez exchange algorithm), the

Butterworth filter was chosen here because it exhibits a flat pass band (no ripple), and is

simple to compute. The general equation for a Butterworth filter is given by

$$|H(\omega)| = \frac{1}{1 + \left(\dfrac{\omega}{\omega_0}\right)^{2n}} \qquad (4.15)$$

where n is the order of the filter and ω_0 is the cutoff frequency of the filter. The transition

from the pass band to the stop band becomes sharper as the order increases. The

bandwidth and the cutoff frequencies are chosen based on the signal characteristics.

In eddy current analysis, the filter phase response should ideally be a zero-phase

response. This is essential because locating a flaw accurately is also very vital in addition

to detection of flaws. A zero phase filter satisfies the following condition on its impulse response h(n):

$$h_1(n) = h(n) * h(-n).$$

(4.16)

$$H_1(\omega) = |H(\omega)||H(-\omega)|e^{j\theta(\omega)}e^{j\theta(-\omega)}$$

(4.17)

$$\Rightarrow H_1(\omega) = |H(\omega)|^2$$

(4.18)

h(n) must be real. It is non-causal and can only be used if the application data is stored and accessible at later time, as in this case.

4.4.3 Continuous Wavelet Transform (CWT)

The wavelet transform is the third approach investigated for signal enhancement. Wavelet transforms are multi-resolution representations of signals and images. The transform decomposes signals and images into multiple scales, and is used in a variety of applications including data compression and denoising.

The most commonly used transform in analysis of data is the Fourier transform [32, 40] given by

$$F(\omega) = \frac{1}{2\pi} \int_{-\infty}^{\infty} f(t)e^{-j\omega t} dt.$$

(4.19)

where $f(t)$ is the time domain signal, and $F(\omega)$ is its Fourier transformation. However, in the Fourier domain, time information about the input signal is lost [32, 40], and therefore, it can only be used for stationary signals whose frequency components do not vary over time. For this reason, the Fourier transform is usually not used with non-stationary signals.

Time-frequency methods such as the short time Fourier transforms (STFT) [32] and wavelet transforms [41, 42] are better suited for the analysis of such signals. The short time Fourier transform gives a localized Fourier transform given by

$$STFT(\tau, \omega) = \int_{-\infty}^{\infty} f(t)g(t-\tau)e^{-j\omega t}dt \qquad (4.20)$$

where $g(t\text{-}\tau)$ represents the time domain window centered at τ .

The resolution in time and frequency remains the same for all frequencies using the STFT. This, in turn, makes STFT unsuitable for signal analysis where low frequency components are spread out in time and high frequency components are concentrated in time. In such cases, a sharper time resolution with smoother frequency resolution window is need for higher frequency components.

The wavelet transform performs multi-resolution analysis of signals using varying window sizes. There is a trade-off between resolution in time and resolution in frequency. The continuous wavelet transform is defined as [32, 42]

$$\psi_x^{\varphi}(\tau, s) = \frac{1}{\sqrt{|s|}} \int x(t)\varphi * \left(\frac{t-\tau}{s}\right) dt . \qquad (4.21)$$

The transformed signal $\psi_x^{\varphi}(\tau, s)$ is a function of two variables, τ and s, representing the translation and scale parameters respectively. $\varphi(t)$ is the mother wavelet (transforming function), which can be considered as a band pass function centered around some center frequency and translated in time to select the part of the signal to be analyzed [32, 41, 42]. The contribution of the wavelet to a signal is given by inner products of the dilated and translated versions of the mother wavelet with the signal. Hence the wavelet transform represents the correlation between the signal and a scaled version of the mother
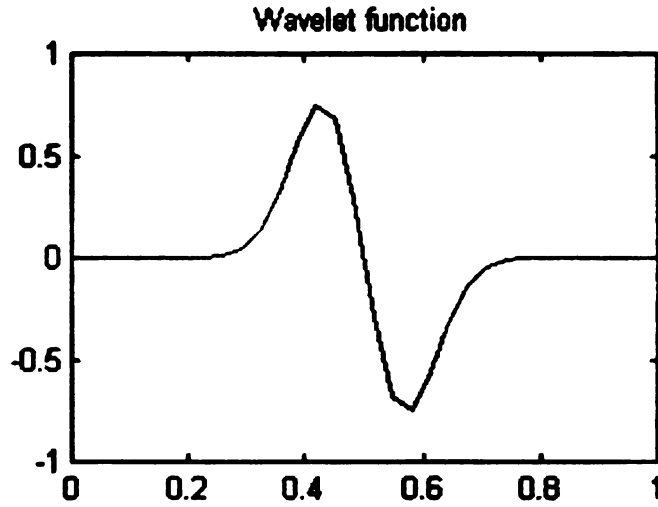
Figure 4.6 Gaussian wavelet (scale 6, order 1)

wavelet. A Gaussian mother wavelet of order one, given by Eq.(4.22), is used in this study as the mother wavelet:

$$g(x) = -2xe^{-x^2}.$$ (4.22)

4.5 Adaptive Threshold for Detection

Although the preprocessing stages enhance the signal to noise ratio significantly in various regions of the steam generator tubes, there are usually unwanted artifacts still present in the data. The application of a threshold on both amplitude and phase is a simple method for identifying flaw indications. Thresholding is a well known technique and many threshold selection methods have been proposed in the literature [9, 36, 37]. The techniques have varying accuracy and one of these techniques may be selected depending on the application.

Conventional thresholding uses a global threshold for the data. Hard thresholding sets signals less than the threshold to zero while soft thresholding subtracts the threshold

from the data [36]. This technique is good as long as the noise content over varied data sets is similar and the threshold can be a fixed quantity. This condition is not common in eddy current data analysis where the noise levels can vary significantly. In such cases conventional thresholding fails to detect flaws and a thresholding technique that has the capability to change the threshold dynamically is required [36, 38].

The use of an adaptive threshold alleviates some of the problems with changing noise conditions between different data sets. Adaptation of the threshold is achieved by using the mean μ and variance σ^2 of data x, which are computed using

$$\mu = mean(x) \tag{4.23}$$

$$\sigma^2 = \mathrm{var}iance(x). \tag{4.24}$$

The threshold T is then calculated as

$$T = \mu + n * \sigma \tag{4.25}$$

where the choice of the multiplicative factor n is heuristic. Data below the threshold is set to zero. This threshold changes with changing conditions in the input data and enables the separation of potential flawed indications from noise.

4.6 Feature Extraction and Classification

As described in the previous section, an adaptive threshold locates all the potential flawed indications in steam generator inspection. However, not all of these indications are true flaws, and a classification algorithm is necessary to identify defects from non-defects, and further classify defects according to degradation types. Classifications algorithms with high detection and low false alarm rates are usually desired.

As a first step to classification, a mapping is obtained from signal space to a feature space. A feature is a distinguishing attribute of a signal [43], and features are computed from the signal based on various parameters. The goal is to extract and compact information in the signal into a small set of features such that the features enhance the amount of discriminatory information and eliminate redundancy in the data. These features are then used in a classification algorithm, which maps from feature space to a decision space with a finite number of categories [36].

Feature based signal classification techniques are commonly used in many applications. An overview of the classifier scheme used in this study is shown in Figure 4.7.

Classification can be complex in many cases because the relation between the parameters of interest and the signal (image) may not be clear. In many cases, classes cannot be distinguished by use of a single feature. Suitable features need to be extracted and the process is very problem dependant. Feature extraction deals with extracting relevant information from the input signals, and many statistical and physical features can be computed. These include amplitude-based features such as the mean, standard deviation, energy, entropy and eigen values, and shape-based features such length, area, size etc. In image processing, texture, color and geometric features can also be calculated [37]. Once a set of features have been computed, an optimal set of features that can classify the signals with minimal errors have to be identified. A variety of optimal feature
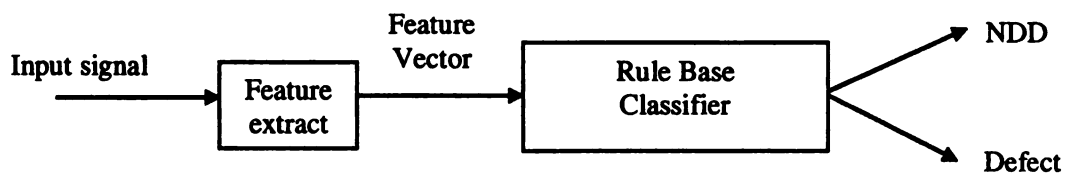

Figure 4.7 Classification

66

identification algorithms such as linear discriminant analysis (LDA) [36], principal component analysis (PCA) [36] and iterative dichotomizer 3 (ID3) [32] may be used for this purpose.

These features are then input to a classifier for identifying defects and separating them from non-defects. Commonly used classification techniques include minimum distance-based classification, maximum likelihood classification, neural network based classifiers, support vector machines and rule based classifiers [36]. A rule base classifier is employed here. A rule-based classifier classifies the data by following a set of rules. These rules are determined by analysis of a set of training signals, and the rules can be very data dependant. Once the rules are developed using the optimal number of features, they can be used to distinguish between various degradation mechanisms (Figure 4.7). In this study, the features computed include

1. Maximum, minimum, mean values of the real and imaginary components.

2. Maximum, minimum, mean values of the amplitude and phase of the eddy current signal. The amplitude and phase are computed as

$$M = \sqrt{x^2 + y^2} \qquad\qquad (4.26)$$

$$\phi = \tan^{-1}\left(\frac{y}{x}\right) \qquad\qquad (4.27)$$

where x and y are the real and imaginary components of the eddy current signal. These features are computed because they describe the eddy current signal and give sufficient discriminatory information between defects and non defects.

The ID3 algorithm is used in this study to develop the rules. A set of training samples which best describe an event to be classified (defect or non-defect) are collected

[43, 44]. Attributes that are most informative must be used in order to find a simple decision process that correctly classifies the training data and also has a high classification performance on the test data. Such features help in finding a decision tree with maximum information and minimum tests. The selection of tests for maximum information gain in classification is based on information theory [43, 44]. The information content in a message m_i is given by

$$I(m_i) = -\log_2 p(m_i).$$ (4.28)

The expected information in a set of n messages (M) is given by

$$I(M) = \sum_{i=1}^{n} - p(m_i) \log_2 p(m_i)$$ (4.29)

where $p(m_i)$ is the probability of each message.

This concept is used to build a rule-base or decision process which conveys information about the classification. Consider a set of Q instances partitioned into N disjoint classes $(A_1, A_2, \ldots\ldots A_N)$. Then the information content needed to make a decision that $x \in Q$ belongs to a class A_j is given by

$$I(A_j) = -\log_2\left(\frac{|A_j|}{|Q|}\right)$$ (4.30)

where $|A_j|$ is the number of instances in the subset A_j and $|Q|$ is the total number of elements. The expected information of a message [32] identifying a class of a random instance $x \in Q$ is

$$I(T) = -\sum_{j} \frac{|A_j|}{|T|} \log_2\left(\frac{|A_j|}{|T|}\right).$$ (4.31)

This is the entropy of Q and measures the average information needed to identify the class of instances in Q.

After the thresholding operation, potential indications are obtained as regions of interest (ROI) in the data. Features are computed for each ROI and are applied to an ID3 algorithm to both determine those features that have maximum discriminatory information, and develop the rules. These rules are then used to classify the ROIs as defects and non-defects.

CHAPTER 5. RESULTS AND DISCUSSION

In the previous chapters, the concepts of nondestructive evaluation, eddy current phenomena and probes, finite element modeling, artificial neural networks and signal processing algorithms were discussed. This chapter describes the results obtained on application of an axi-symmetric finite element model to the prediction of eddy current probe signals obtained in steam generator tubing using array probes and the development of compensation and analysis algorithms for the array probe eddy current data collected from steam generator tubes. The results of the implementation are presented and discussed.

5.1 Database Description

Two databases were used to evaluate the analysis algorithms along with a third simulation database to evaluate compensation algorithms. All databases contain eddy current data from steam generator inspection. A brief description of these databases is given below.

5.1.1 Laboratory Database

The first database was the ETSS database, which is generated by the Electric Power Research Institute. This database consists of 7 array probe eddy current data files collected at excitation frequencies of 100, 200, 300 and 400 kHz. The signals contained a total of 14 defects (both axial and circumferential cracking). All signals were calibrated initially and defects in tube support plate regions were analyzed.

5.1.2 Field Database

The second database is a field database collected from a live steam generator. The data consists of 199 files collected at excitation frequencies of 70, 190, 380 and 750 kHz. Each file consists of eddy current data from 70' long straight tubes. While the data had signals from both tube support plates as well as free span regions (the region between support plates), data from only the free span regions was analyzed here. Table 5.1 summarizes the number of channels, and the probe types used for both the laboratory and field databases.

Table 5.1: Different array probes and channels in each probe

	# of coils in array probe	Total # of channels	Laboratory / Field data
Probe 1	16*3	32*4+32*4=256	Laboratory Data
Probe 2	16*2	32*4+16*4=192	Field Data
Probe 3	14*2	28*4+14*4=168	Field Data

5.1.3 FEM Simulation Database

The third database used is generated using a finite element model. The geometry that is simulated is of a transmit-receive probe close to an Inconel 600 tubing with defects at multiple depths (40% 60% 80% and 100% Inner diameter and Outer diameter), with the transmit coil excited at multiple frequencies (100kHz, 200kHz, 300kHz and 400kHz). The two dimensional field problem is assumed to be axi-symmetric.

Figure 5.1 shows the transmit-receive coil configuration placed close to an Inconel 600 tubing. The transmit coil is excited with a uniform current density of 10^3A/m^2. Because of the symmetry about the vertical axis, it is enough to apply the finite
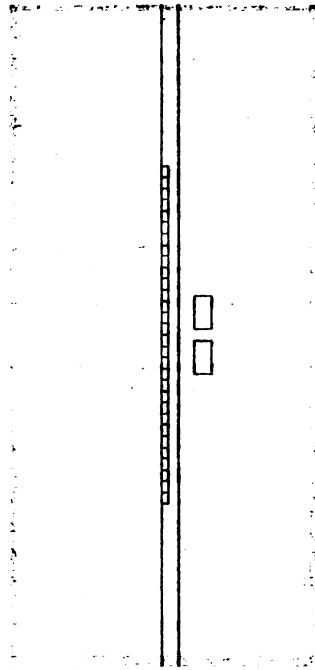
71

Figure 5.1: 2D FEM of transmit-receive coil configuration and Inconel tubing

element analysis to one half of the region. The discretization is done using a generalized

automatic mesh generator using FEMLAB ([45]).

The objective is to calculate the magnetic vector potential in the region using

finite element model and from this, to calculate the induced voltage in the receiver coil at

multiple excitation frequencies for different depths of defects, and different coil

locations.

5.2 Simulation Results

5.2.1 Simulation Parameters

The material properties used in the finite element modeling are given in Table 5.2 while

the tube and coil dimensions are provided in table 5.3.

Table 5.2 Material properties

Material	Electrical Conductivity σ (Ω/m)	Relative Permeability μ_r
Copper	5.77×10^7	1
Inconel 600	1×10^6	1

Table 5.3 Coil and tube dimensions

Quantity	Dimension (mm)
Length of tube	60
Outer diameter of the tube	19
Inner diameter of the tube	16.7
Length of the defect	7
Coil dimensions (transmit and receive coils)	3x1

The geometry shown in Figure 5.1 was used to conduct simulations to obtain complex induced voltage trajectories. Multiple models were developed to collect data for multiple defects at multiple frequencies and multiple liftoffs. Table 5.4 shows the various parameters that were considered to develop the models. Each combination of the different parameters (for instance, 40% deep I.D. flaw with excitation frequency 100 kHz and liftoff 3 mm) was used to generate data.

Table 5.4 Simulation parameters

Depth (%)	Types of defects	Excitation frequency (kHz)	Liftoff (mm)
40	I.D.	100	0.5
60	O.D.	200	1.0
80		300	1.5
100		400	2.0
			2.5
			3.0

Figure 5.2(a) shows an example of the impedance plane diagram of a 60% O.D defect at 100 kHz, at a liftoff of 0.5mm from the tube.

5.2.2 Results of Simulation

The simulated data was calibrated using the 60% O.D. Defect. The signal from the 60% O.D. flaw is rotated to 90° and scaled to a 1 V p-p at all frequencies. All the other defects were rotated and scaled accordingly. Figure 5.2 (a), (b) show the calibration operation on the simulated signals. Figure 5.2 (a) presents the original signal from a 60% O.D. flaw, while Figure 5.2 (b) shows the result of calibration. Figure 5.3 shows the real and imaginary components of the signal in Figure 5.2 (b), after calibration. The liftoff in this case was at 0.5 mm, and the excitation frequency was 100 kHz.
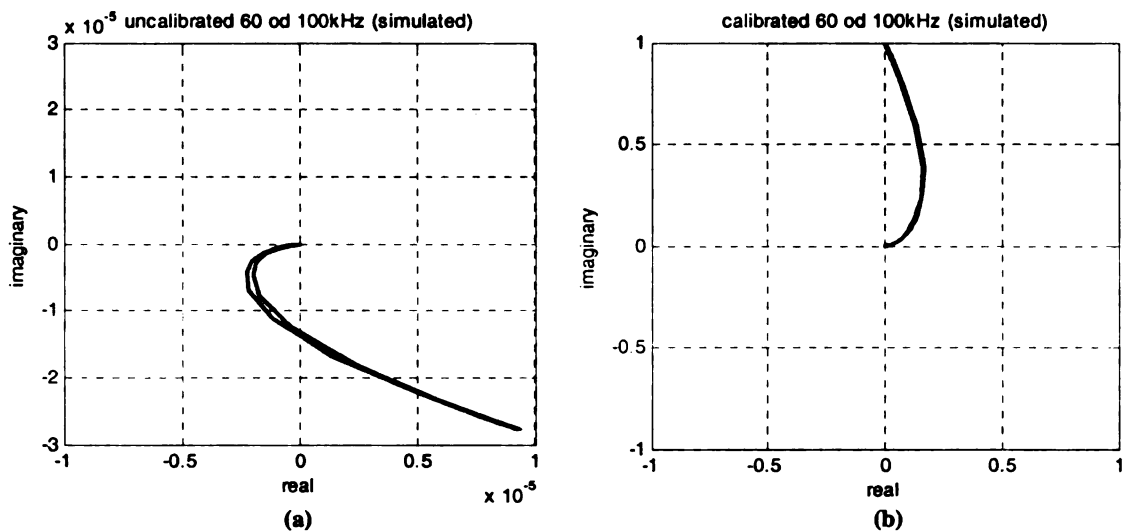
Figure 5.2 Flaw 60% O.D. at 100 kHz (a) simulated (uncalibrated) (b) simulated (calibrated)
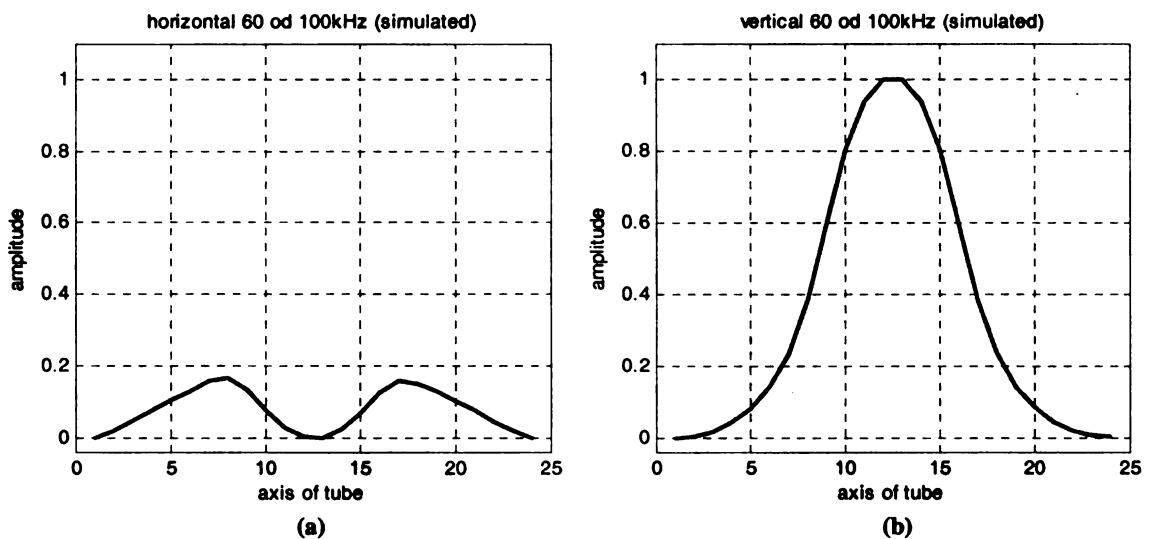
Figure 5.3 Simulated flaw 60% O.D. at 100 kHz (a) horizontal component (simulated) (b) vertical component (simulated)
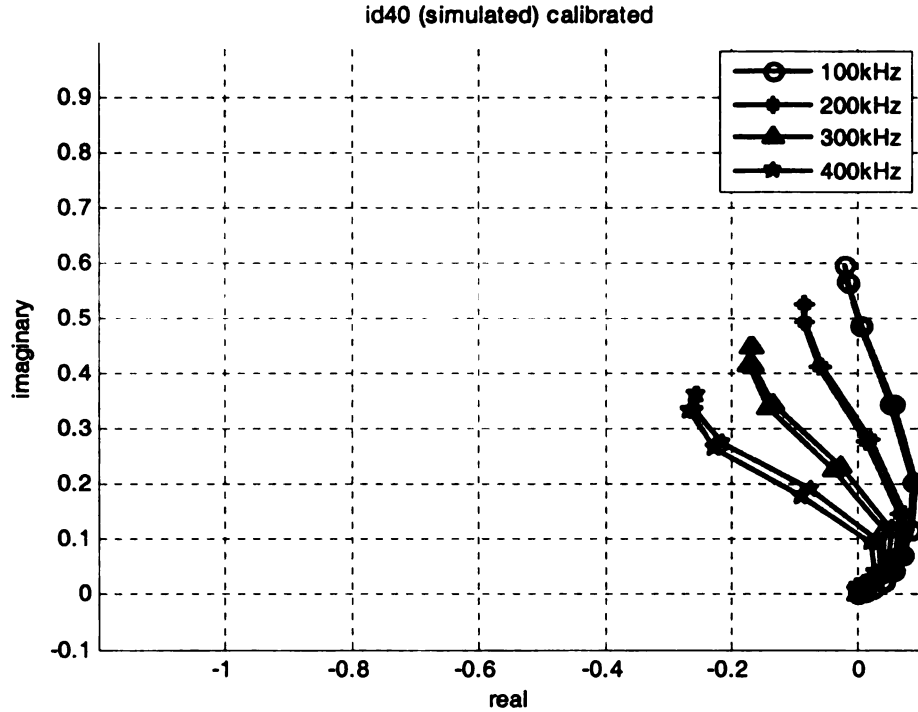
Figure 5.4 Simulated flaw 40% I.D. at multiple frequencies (simulated)

The results of simulation at four different frequencies (100 kHz, 200 kHz, 300 kHz and 400 kHz) are shown in Figure 5.4 for a 40% I.D. flaw. As seen from the figure, the phase angle of the signal changes with excitation frequency, and this property may give additional information in the design of compensation and analysis algorithms.

Figure 5.5 shows defects at various depths obtained at 400 kHz. Figure 5.5 (a) shows several I.D. defects while Figure 5.5 (b) shows O.D. defects. Figure 5.6 shows a 40% I.D. defect at 200 kHz at multiple liftoffs. These results indicate that the signal behavior with depth, excitation frequency and liftoff change is similar (change in phase and magnitude), and underscores the need for compensation algorithms. The results of these algorithms are described next.
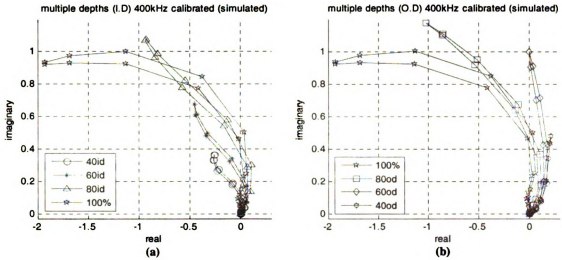
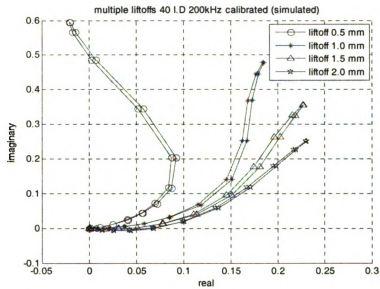**Figure 5.5 Simulated defects of various depths at 400 kHz**

Figure 5.6 Defect 40% id at multiple liftoffs

5.3 Compensation Results

5.3.1 Affine Transformations

Affine transformations are investigated to compensate for liftoff. Two sets of transformation parameters were computed based on a single frequency, and dual frequencies to achieve compensation. In the first approach, a transformation matrix is computed by using signals at liftoffs 1 mm, 2 mm and 3 mm and transforming them to minimum liftoff (0.5 mm) for the same frequency. A 48x48 transformation matrix is obtained, and these parameters are then applied to test signals at intermediate liftoffs of 1.5 mm and 2.5 mm. The results are shown in Figure 5.7. Figure 5.7 shows the affine transformation results for a 60% I.D. at 400 kHz. The lift offs in Figures 5.7 (a) and (b) are used to compute the transformation parameters as described in chapter 3 and Figure 5.7 (c) and (d) show the test results with intermediate liftoffs.

Similarly, Figure 5.8 shows the affine transformation results for a 60% I.D. whose parameters are computed using data at two frequencies (100 and 200 kHz). The lift offs in Figure 5.8s (a) and (b) are used to compute the transformation parameters and Figures 5.8 (c) and (d) show the test results with intermediate liftoffs. Both sets of results indicate that the affine transformation is capable of accurately compensating for liftoff. Additional results are summarized in Tables 5.5 and 5.6.
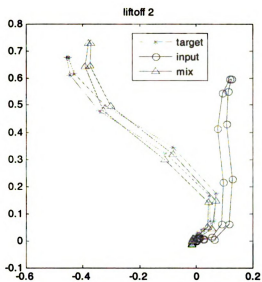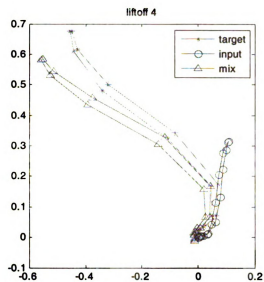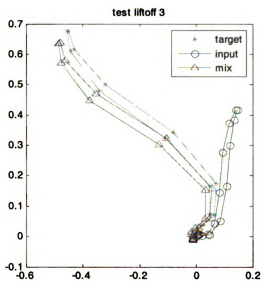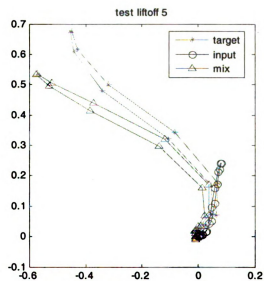
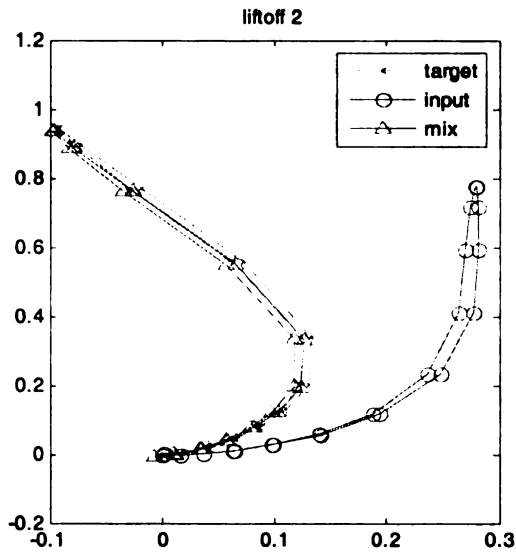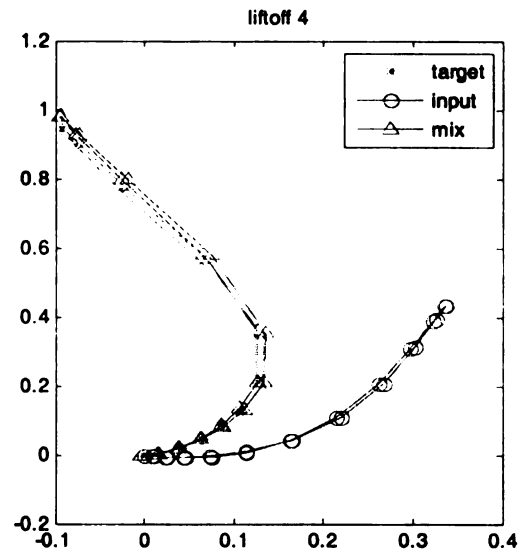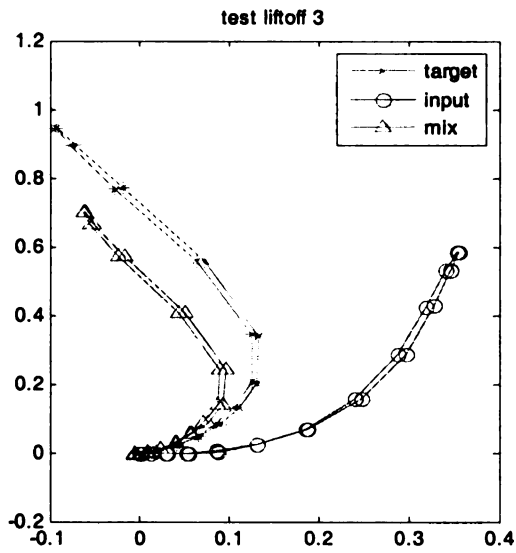**Figure 5.7 Affine transformation results on 60% id at 400kHz (single frequency) (a) liftoff 1mm (b) liftoff 2 mm (c) test liftoff case 1.5mm (d) second test liftoff case 2.5mm**
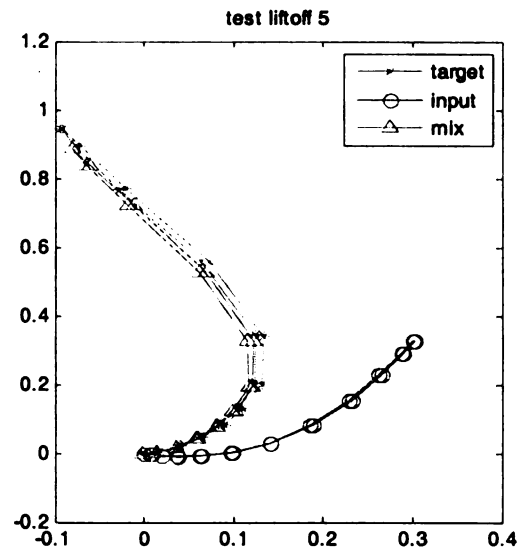
Figure 5.8 Affine transformation results on 60% id using dual frequency (100kHz-200kHz) (a) liftoff 1mm (b) liftoff 2 mm (c) test liftoff case 1.5mm (d) second test liftoff case 2.5mm

5.3.2 Multilayer Perceptron

In this technique, multiple neural networks are developed for compensation at each frequency. Since four excitation frequencies were used, for the single frequency case, four MLPs are generated, and the results are shown in Figure 5.9 and 5.10. Figures 5.9 (a) and (b) present the signals used to train the multilayer perceptron and Figure 5.9 (c) and (d) show the test results with intermediate liftoffs. Likewise, Figure 5.10 shows the results when using data at two frequencies (100 and 200 kHz) for training. In both figures, a 60% I.D. flaw was used. Again, the results indicate the viability of the proposed approach.

5.3.3 Radial Basis Function Networks

Finally, Figures 5.11 and 5.12 show the results of suing an RBF neural network for compensation. Again, as in earlier cases, Figure 5.11 shows the results of single frequency compensation for a 60% I.D. flaw, and Figure 5.12 shows the results for a two-frequency (100 kHz and 200 kHz) approach to compensation.
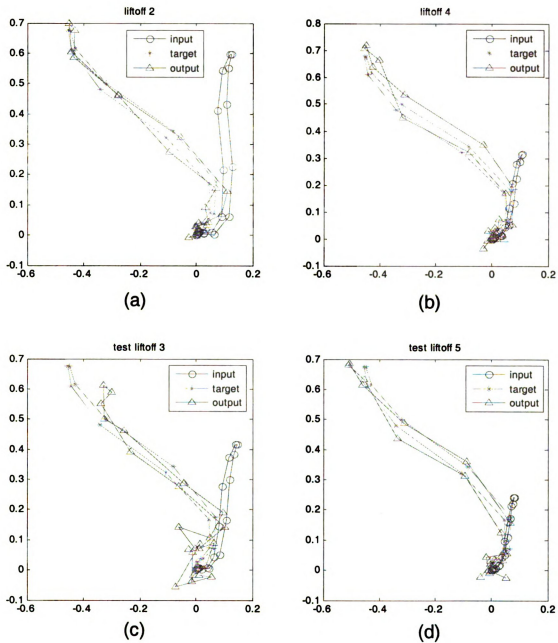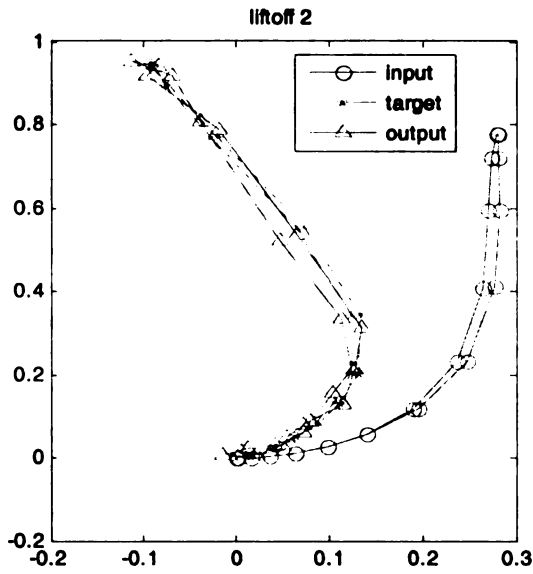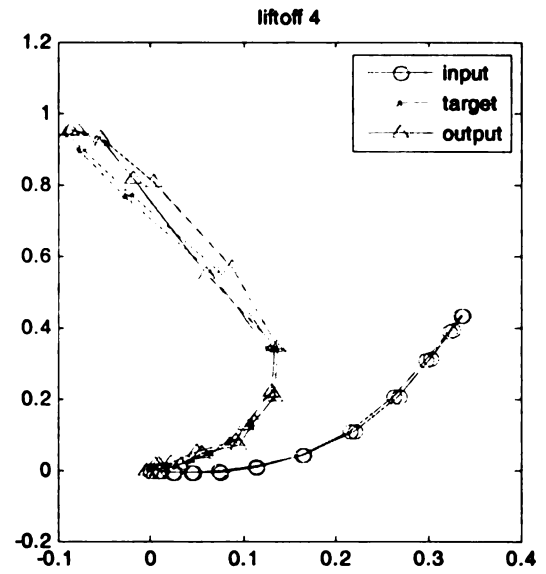
Figure 5.9 **MLP results on 60% id using single frequency (400kHz) (a) liftoff 1mm (b) liftoff 2 mm (c)
test liftoff case 1.5mm (d) second test liftoff case 2.5mm**

Figure 5.10 MLP results on 60% id using dual frequency (100-200kHz) (a) liftoff 1mm (b) liftoff 2 mm (c) test liftoff case 1.5mm (d) second test liftoff case 2.5mm
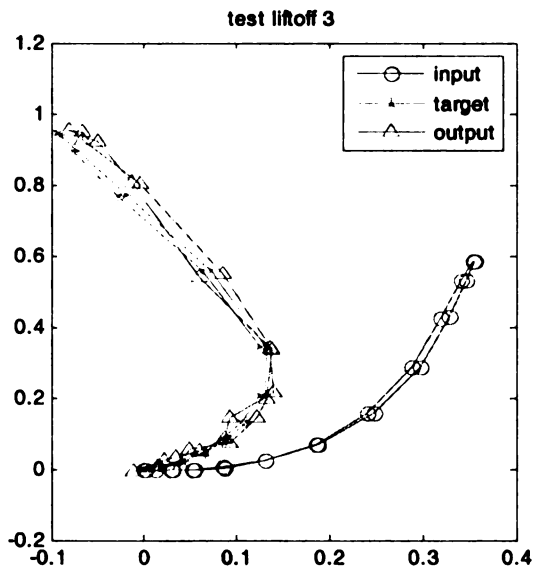
Figure 5.11 RBF network results on 60% id using single frequency (400kHz) (a) liftoff 1mm (b) liftoff 2 mm (c) test liftoff case 1.5mm (d) second test liftoff case 2.5mm
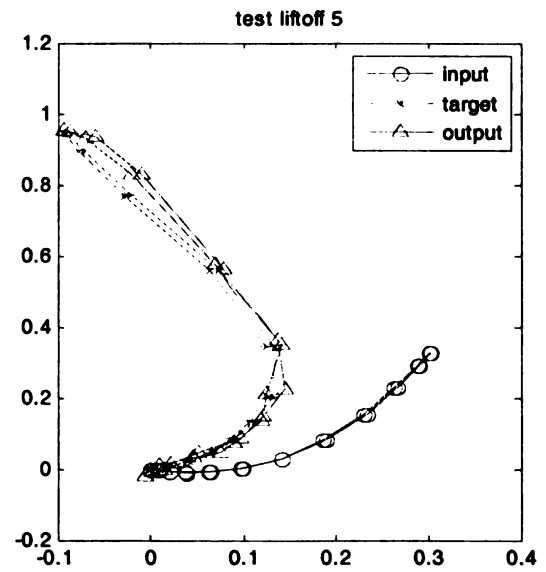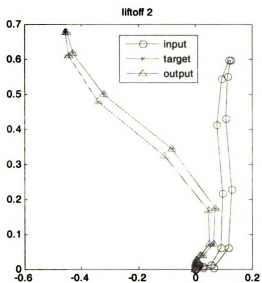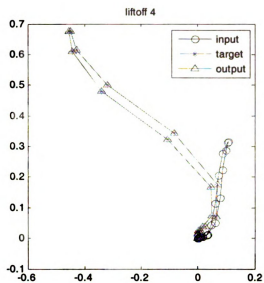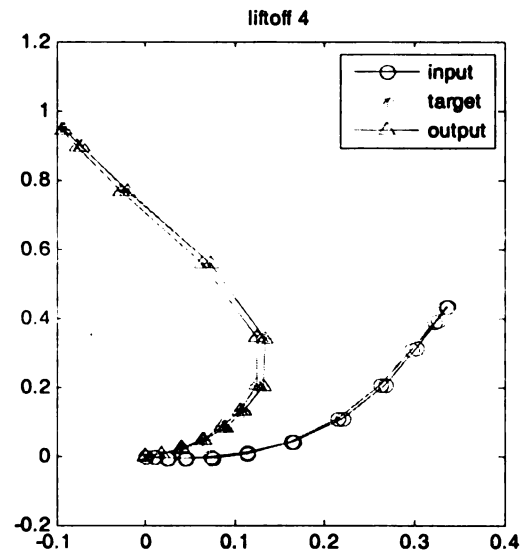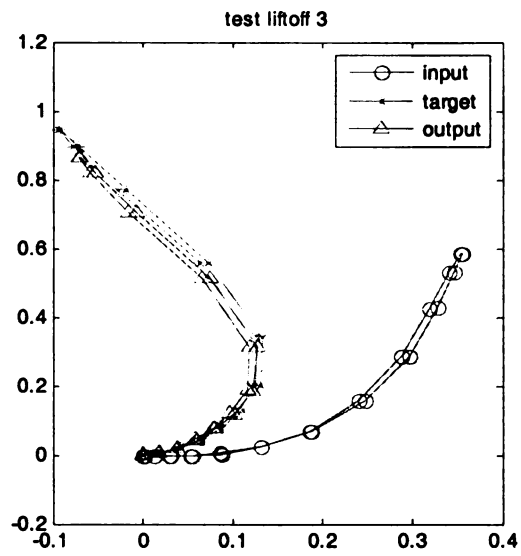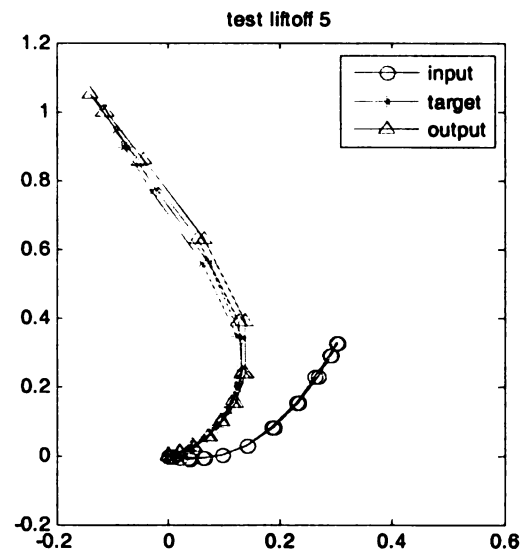
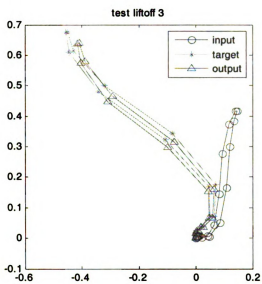**Figure 5.12 RBF network results on 60% id using dual frequency (100-200kHz) (a) liftoff 1mm (b) liftoff 2 mm (c) test liftoff case 1.5mm (d) second test liftoff case 2.5mm**
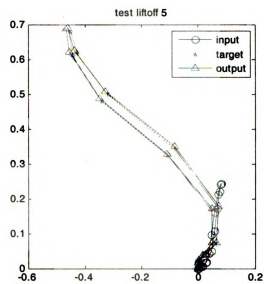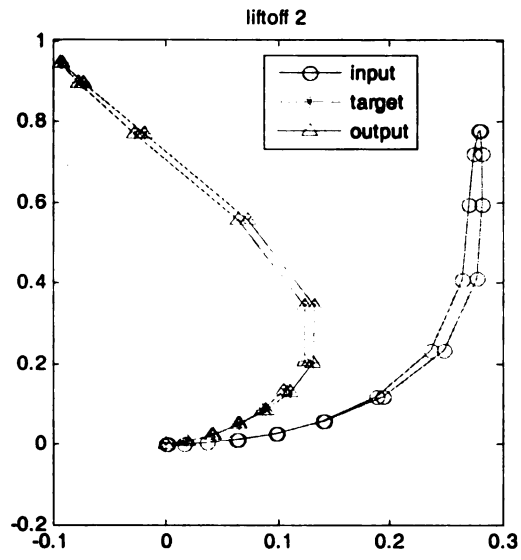
The results of the three compensation techniques are summarized in Tables 5.5 and 5.6. Table 5.5 presents the results for the single frequency case and Table 5.6 for the two frequency case. The metric used to compare the results between the three techniques is the root mean square error given by

$$X_c = \begin{bmatrix} H_c \\ V_c \end{bmatrix} \tag{5.1}$$

$$X_d = \begin{bmatrix} H_d \\ V_d \end{bmatrix} \tag{5.2}$$

$$E = \|X_d - X_c\| \tag{5.3}$$

$$E = \frac{1}{N}\left\{\sum_{i=1}^{N}\left[(H_d{}^i - H_c{}^i)^2 + (V_d{}^i - V_c{}^i)^2\right]\right\}^{\frac{1}{2}} \tag{5.4}$$

Table 5.5 Comparison of single frequency compensation (100 kHz)

Depth (%)	Affine Tx		MLP		RBF	
	Train (*1e-3)	Test	Train	Test	Train (*1e-3)	Test
40 I.D.	0.1209	0.0058	0.0023	0.0263	0.0020	0.0050
60 I.D.	0.0958	0.0039	0.0233	0.0277	0.0031	0.0265
80 I.D.	0.0386	0.0093	0.0036	0.0122	0.0051	0.0140
100	0.0771	0.0049	0.0527	0.0537	0.0062	0.1542
80 O.D.	0.0543	0.0115	0.0030	0.0372	0.0025	0.0134
60 O.D.	0.0483	0.0044	0.0247	0.0267	0.0064	0.0190
40 O.D.	0.0768	0.0019	0.0030	0.0089	0.0029	0.0062
Average	0.0731	0.0059	0.0161	0.0275	0.0040	0.0341

where H_d and H_c are the horizontal components and V_d and V_c are the vertical components of the desired output and the actual output respectively. The training and test results for the single frequency case are presented in table 5.5 for the three techniques. From Table 5.5, the affine transformation is seen to yield the minimum error when compared to the other two techniques.

Similarly, Table 5.6 shows the results for the compensation using data at two frequencies. Again, the affine transformation is seen to give the best results. The reason for the superiority of the affine transformation may be the high complexity of the neural networks used (large number of parameters). This in turn requires a large amount of data for training the neural network, something lacking in this study. Therefore, these results may depend on the availability of a larger database for training. This aspect will be

Table 5.6 Comparison of two frequency compensation (100 kHz- 200 kHz)

Depth (%)	Affine Tx		MLP		RBF	
	Train	Test	Train	Test	Train (*1e-3)	Test
40 I.D.	0.0047	0.0136	0.0041	0.0187	0.0059	0.0108
60 I.D.	0.0034	0.0195	0.0046	0.0057	0.0105	0.0083
80 I.D.	0.0036	0.0121	0.0236	0.0252	0.0063	0.0267
100	0.0059	0.0244	0.0528	0.0534	0.0133	0.1489
80 O.D.	0.0062	0.0186	0.0253	0.0422	0.0214	0.0301
60 O.D.	0.0052	0.0109	0.0066	0.0098	0.0073	0.0187
40 O.D.	0.0086	0.0087	0.0042	0.0166	0.0065	0.0159
Average	0.0054	0.0154	0.0173	0.0245	0.0102	0.0371

investigated further.

5.4 Signal Processing

5.4.1 Suppression

Figure 5.13 shows the results of median suppression as a method for support suppression on data consisting of flaws in the support region. Figure 5.13(a) shows the data before support suppression and Figure 5.13(b) shows the result after support suppression. The defect and the support have similar range of amplitudes; however, support suppression is seen to enhance the defect significantly.

Mixing was also performed on the calibration data and the transformation parameters were saved, and applied to field data. Typical support suppression results using mixing are shown in Figure 5.14. Figure 5.14(c) shows the support-suppressed
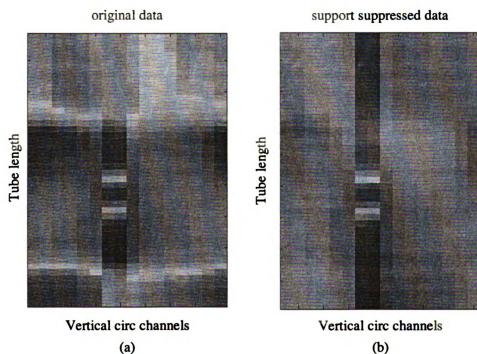
Figure 5.13 Support suppression (a) before suppression (b) after suppression

| axial 300 kHz | axial 200 kHz | 300-200 kHz mix |
| (a) | (b) | (c) |
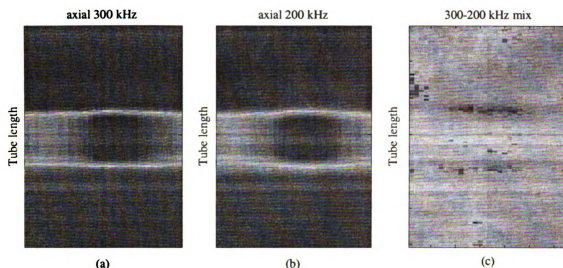
Figure 5.14: Mixing (a) support from raw data at 300kHz (b) support from raw data at 200kHz (c) 300kHz-200kHz mix channel

signal. It can be clearly noticed that a majority of the support signal is suppressed. Thus, signal suppression is vital if the signals of interest are to be observed. Both techniques are

Table 5.7 Median suppression and mixing results

| Lab Data Group | Total # of flaws in 7 tubes | Median suppression | | Mixing | |
		Flaws detected	False calls	Flaws detected	False calls
1	2	2	2	2	2
2	4	2	2	2	0
3	2	2	7	2	0
4	3	3	2	3	0
5	3	3	0	3	0
TOTAL	14	12	13	12	2

good for supports that encircle the tube completely. In the case of broached supports however, these techniques would fail as the support signal is not present in all channels. Table 5.7 summarizes the results from median suppression and mixing, and indicates that mixing algorithms are superior to median suppression.

5.4.2 Filtering and Denoising

Depending on the utility, steam generator tubes can be of different types. Examples include straight sections, square bends and U-bends. U-bend data can be significantly different from the straight leg free span or support region data as shown in Figure 5.15. The algorithms used for analyzing U-bend therefore will be different from those used for free span straight tubes. Thus, location specific and plant specific algorithms are necessary to optimally analyze array probe eddy current data. For instance, most U-bend data has periodic noise. Further, noise levels in the intrados and extrados regions were also different. Noise levels at transition regions are also typically high due to geometry changes of the tube where the probe enters or leaves the bend. All these factors have to be considered in designing appropriate filters for noise reduction and signal enhancement.

5.4.2.1 Median Filter

Median filtering removes a substantial amount of noise, and enhances the signal level significantly. However, the filter response is dependant on the size of the window Circumferential cracks are relatively easy to handle because of the fact that the length of the cracks is very small in the axial direction, and the fitler successfully enhances such crack signals. Axial cracks, on the other hand, have significant length and cannot be directly processed by a median filter. If the window size is less than the crack length, the

crack signal will also be eliminated by filtering. However, increasing the length of the window reduces the smoothening effect of the filter.

Figure 5.15 shows the typical response of a median filter. If a signal is computed by using the median values in a constant window from an original signal, the low frequency component is removed and the high frequency signals of interests can be retained.
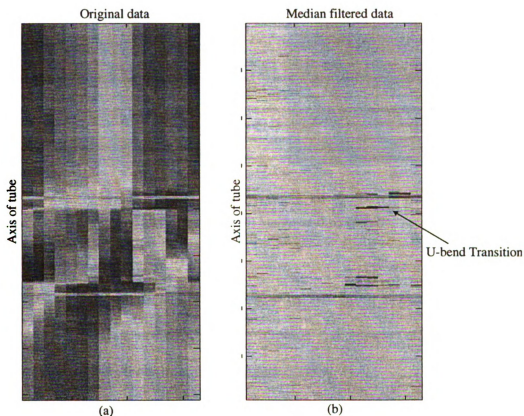
Figure 5.15 Median filtering results (a) original data (b) median filtered data
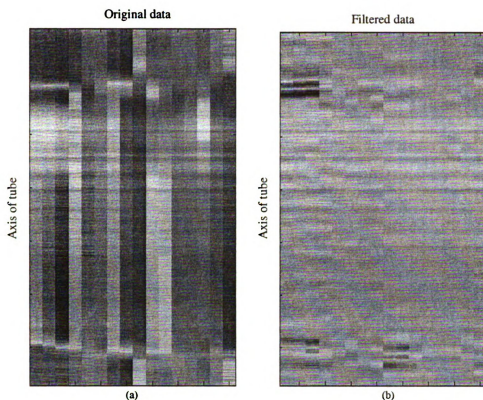
Figure 5.16 Bandpass filter results (a) raw data (b) bandpass filtered data

5.4.2.2 Bandpass Filter

The band pass filter can also be used to remove noise as shown in Figure 5.16. Figure 5.16(a) shows the raw data with the intrados and extrados effects in the U-bend region. These are reduced considerably in Figure 5.16(b).

5.4.2.3 Continuous Wavelet Transform (CWT)

The continuous wavelet transform is another method investigated for signal enhancement. A Gaussian wavelet of order one is used at scale 6 to compute the CWT coefficients. At this scale the support is not suppressed completely but the free-span region of steam generator tube is significantly enhanced. Figure 5.17(b) shows the CWT data of the full-length tube. The free span and support regions are then isolated using

automatic support detection algorithms and processed to detect the defects as shown in

Figure 5.17 (c).
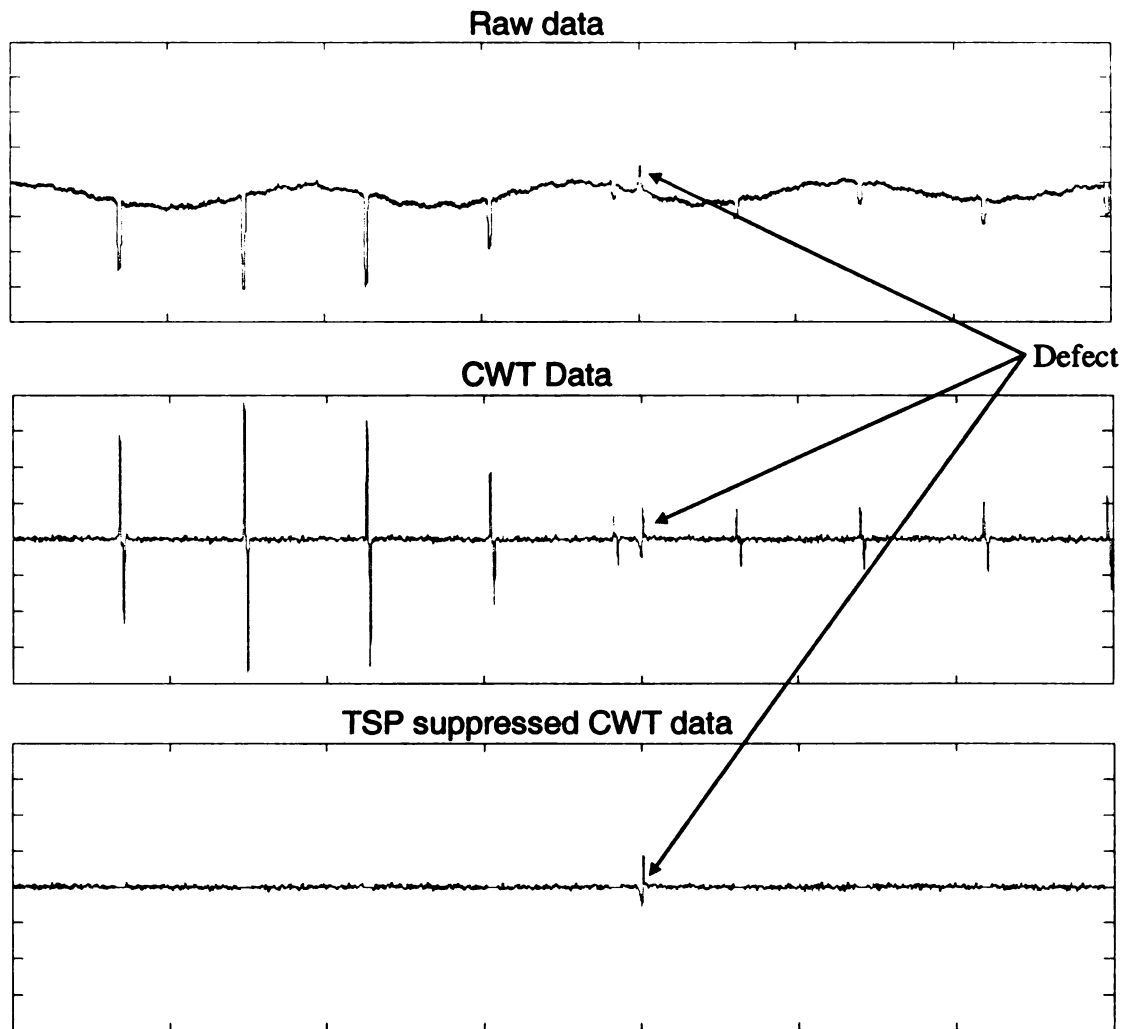
Figure 5.17 CWT (a) raw data (b) CWT data (c) CWT data after TSP removal

5.4.3 Detection Results

Although all the preprocessing steps enhance the signal to noise ratio significantly in various regions of the steam generator tubes, there are some unwanted artifacts present in the data and, hence thresholding of data was used to identify potential flaw indications. Table 5.8 presents a summary of the data available in the two databases. The detection results on both laboratory as well as field data are presented in Tables 5.9 and 5.10.

Table 5.8 Summary of data and algorithms used

Data Set	# of tubes	# of defects	Types of defects	Types of structures	Algorithms used
Lab Data	7	14	Axial and Circumferential cracks	TSP (360°) Drilled supports	Mixing, Median suppression
Field Data	199	27	MBM	Broached TSP	CWT

Table 5.9 Laboratory data detection results

Type of Flaw	Ground Truth	Flaws Detected	Misses	False calls
Circ	4	4	0	2
Axial	10	8	2	0
Total	14	12	2	2

Table 5.10 Field data detection results

Type of Flaw	Ground Truth	Flaws Detected	Misses	False calls
MBM	27	27	0	70

5.4.4 Classification Results

All potential indications that are obtained after the preprocessing are examined to determine if they are defects or non-defects. The objective is to automatically classify the potential indications into defects and non-defects. A rule based classifier was developed for classification of these regions of interest (ROI). Tables 5.11 and 5.12 show the classification results on the lab data and field data sets. The lab data set contains a total of 14 flaws (10 Axial and 4 circumferential flaws) and most flaws were correctly identified. However, two flaws were missed due to very low amplitudes of the defect signals. Note that these two flaws were missed during the preprocessing stage.

Table 5.11 Classification (Laboratory data)

Type of Flaw	Ground Truth	Flaws Detected	Misses	False calls
Circ	4	4	0	2
Axial	10	8	2	0
Total	14	12	2	2

Table 5.12 Classification (Field data)

Type of Flaw	Ground Truth	Flaws Detected	Misses	False calls
MBM	27	27	0	23

Further, results on thee second database indicate that the proposed algorithms can significantly reduce false calls, while giving good detection performance. These results need to be validated on additional data, with other types of flaws.

CHAPTER 6. CONCLUSIONS

This thesis described the development of automated compensation and classification algorithms for array probe eddy current NDE data obtained in the inspection of steam generator tubing. Affine transformations and neural network (MLP and RBF) based methods have been proposed for the liftoff compensation. Additionally, various signal and image processing algorithms have been investigated for defect detection and classification in array probe eddy current data.

The first step in the analysis of array probe data was the development of a numerical model to better understand the array probe inspection process. A 2D axi-symmetric finite element model of a transmit-receive eddy current coil configuration in an Inconel 600 steam generator tubing (with defects) was developed. Several different simulations, with different defect depths and excitation frequencies, were performed and the eddy current signals generated were used to develop lift-off compensation algorithms based on affine transformations and neural networks. Compensation algorithms using data at a single frequency were compared with algorithms using data at two frequencies. The results of compensation indicate that, in general, compensation using two (or possibly more) frequencies tends to be better than compensation algorithms that use a single frequency. Furthermore, affine transformations appear to provide the best compensation results among the three approaches investigated. Training time for neural networks is also an important parameter, and here, the RBF network has an edge over the MLP network here.

Various signal processing algorithms were developed that aid in automatic signal classification. The proposed algorithms are very generic, and a subset of these algorithms

97

can be used selectively to process data obtained from different plants. Algorithms including those for support suppression and noise removal were investigated as a part of this study. These algorithms are used to suppress noise, as well as signals from external support structures, and enhance signal to noise ratio to enable easy detection of defects. A simple adaptive threshold is used to identify potentially flawed indications. These indications are further classified using a rule-base classifier. Results of applying the preprocessing and classification algorithms to several data sets indicate that the proposed algorithms are capable of successfully identifying defect regions with minimal false calls. However, the algorithms require data-specific selection of parameters, which requires the presence of a training database.

Future work includes the development of a three dimensional numerical model for steam generator tubing using an array probe. This model can be used to obtain simulated data that describes the problem more closely when compared to data from 2D axisymmetric models. Optimization of the proposed algorithms, as well as the investigation of other classification algorithms, is also necessary. The development of preprocessing algorithms for the suppression of signals from broached supports is also critical. Finally, the validation of the proposed algorithms on additional data, as well as their validation using data from other designs of array probes, is also a priority.

REFERENCES

[1]   X. Cai, *Iterative Blind Deconvolution and its Application to Characterization of Eddy Current NDE Signals*, M.S. Thesis, Iowa State University, 2001.

[2]   D. E. Bray and R. K. Stanley, *Nondestructive Evaluation: A Tool for Design, Manufacturing and Service*, McGraw-Hill Book Company, 1989.

[3]   W. J. McGonnagle, *Nondestructive Testing*, Second Edition, Gordon and Breach Science publishers, Inc, 1966.

[4]   W. E. Schall, *Non Destructive Testing*, Machinery Publishing Co. LTD, 1968.

[5]   R. Palanisamy, *Finite Element Modeling of Eddy Current Nondestructive Testing Phenomena*, PhD Thesis, Colorado State University, 1980.

[6]   Cs. S. Daroczi and A. Gasparics, *"Depth Sensitive Dual-Frequency Eddy Current NDT Measuring Technique,"* Electromagnetic Nondestructive Evaluation (II), IOS Press, pp. 17-23, Sep, 1997.

[7]   *Automated Analysis of Array Probe Eddy Current Data*, EPRI Technical Report, EPRI, Palo Alto, CA: 2003, (Document ID: 1007867).

[8]   K. Arunachalam, P. Ramuhalli, L. Udpa and S. S. Udpa, *"Nonlinear Mixing Algorithm for Suppression of TSP Signals in Bobbin Coil Eddy Current Data,"* Review of Progress in Quantitative Nondestructive Evaluation, D. O. Thompson and D. E. Chimenti, Eds, Vol. 21, American Institute of Physics, pp.631-638, May 2002.

[9]   P.K. Sahoo, S. Soltani, A.K.C. Wong, Y.C. Chen, *"A Survey of Thresholding Techniques,"* Computer Vision, Graphics, and Image Processing, Vol. 41, pp. 233-260, 1988.

[10]   *From NDT Resource Center - A Web Resource*
http://www.ndt-ed.org/EducationResources/CommunityCollege/EddyCurrents/cc_ec_index.htm

[11]   N. Ida, *Numerical Modeling for Electromagnetic Non-Destructive Evaluation*, Chapman & Hall, 1995.

[12]   K. G. Boving (Editor), *NDE Handbook: Nondestructive Examination for Condition Monitoring*, Butterworths, 1989.

[13]   *Automated Analysis of Bobbin Coil Probe Eddy Current Data*, EPRI Technical Report, EPRI, Palo Alto, CA, 2003, (Document ID: 1007865).

[14] S. P. Sullivan, S. P. Smith, and F. L. Sharp, *"Simultaneous Absolute and Differential Operation of Eddy Current Bobbin Probes for Heat Exchange Tube Inspection,"* Amerian Society for Nondestructive Testing, May 2000.

[15] *Automated Analysis of Rotating Probe Eddy Current Data,* EPRI Technical Report, EPRI, Palo Alto, CA, 2003, (Document ID: 1007866).

[16] P. Xiang, S. Ramakrishnan, X. Cai, P. Ramuhalli, R. Polikar, S. S. Udpa and L. Udpa, *"Automated Analysis of Rotating Probe Multi-Frequency Eddy Current Data From Steam Generator Tubes,"* International Journal of Applied Electromagnetics and Mechanics, Vol. 12, pp. 151-164, 2000.

[17] V. S. Cecco, S. P. Sullivan, R. Lakhan, *X-Probe Technology: An Analyst Perspective,* 21st Annual EPRI Steam Generator NDE Workshop, Berkeley, California, 2002.

[18] *X-Probe Training Outline,* RD-Tech Inc.

[19] G. Lafontaine, F. Hardy, J. Renaud and P. Maletter, *X-Probe^{TM} ECT array: A high-Speed Replacement for Rotating Probes,* 19th EPRI Steam Generator NDE Workshop, Monterey California, July, 2000.

[20] L. S. Obrutsky, R. J. Lakhan, S. P. Sullivan, N. J. Watson, *Feasibility of Detecting Stress Corrosion Cracking in Tight-Radius U-bend Sections of I600 SG Tubes,* 21st EPRI Steam Generator NDE Workshop, Berkeley, California, 2002.

[21] P. Dulyakarn, Y. Rangsanseri, and P. Thitimajshima, *Histogram Transformation based Threshold Selection for Image Segmentation,* King Mongkut Institute of Technology, Bangkok.

[22] I. Altpeter, R. Becker, G. Dobmann, R. Kern, W. Theiner and A. Yashan, *Robust Solutions of Inverse Problems in Electromagnetic Non-Destructive Evaluation,* Institute of Physics Publishing, 2002.

[23] H. Iswahjudi and H. H. Gatzen, *"FEM Simulation for Design and Evaluation of an Eddy Current Micro-sensor,"* Proceedings of 14th European Simulation Symposium, 2002.

[24] S. A. Mandayam, *Invariance Transformations For Processing NDE Signals,* PhD Thesis, Iowa State University, 1993.

[25] D. Kim, *A Novel Approach To The Classification of Ultrasonic NDE Signals,* PhD Thesis, Iowa State University, 2002.

[26] H. T. Croft, K. J. Falconer and R. K. Guy, *Unsolved Problems in Geometry,* New York: Springer-Verlag, pp. 3, 1991.

[27] D. M. Bates and D. G. Watts, *Nonlinear Regression and Its Applications*, New York: Wiley, 1988.

[28] E.W. Weisstein, *Nonlinear Least Squares Fitting, From MathWorld--A Wolfram Web Resource*, http://mathworld.wolfram.com/NonlinearLeastSquaresFitting.html

[29] J. E. Gentle, *Gaussian Elimination*, Numerical Linear Algebra for Applications in Statistics, Berlin: Springer-Verlag, pp. 87-91, 1998.

[30] R. P. Lipman, "*An Introduction to Computing With Neural Nets*," IEEE ASSP Magazine, Vol. 4, pp. 4-22, April 1987.

[31] S. Haykin, *Neural Networks: A Comprehensive Foundation*, Macmillan Publishing Company, Englewood Cliffs, NJ, 1994.

[32] M. Seo, *Automated Ultrasound Signal Classification Scheme*, Masters Thesis, Iowa State University, 1998.

[33] S. Katagiri, *Handbook of Neural Networks For Speech Processing*, Artech House, 2000.

[34] M. J. L. Orr, *Introduction to Radial Basis Function Networks, centre for Cognitive Science*, University of Edinburgh, 1996.

[35] R. O. Duda and P. E. Hart, *Pattern Classification and Scene Analysis*, John Wiley and Sons, 1973.

[36] B. Jahne, *Digital Image Processing*, Springer, 2002.

[37] W. K. Pratt, *Digital Image Processing*, John Wiley and sons, 1991.

[38] R. C. Gonzalez and R. E. Woods, *Digital Image Processing*, Prentice Hall, 2002.

[39] K. Lacanette, *A Basic Introduction to Filters*, National Instruments, Application Note 779.

[40] A. V. Oppenheim, and R. W. Schafer, *Discrete-Time Signal Processing*, Prentice Hall, 1989.

[41] M. Vetterli and J. Kovacevic, *Wavelets and Subband Coding*, prentice Hall, 1995.

[42] E. Hernandez and G. Weiss, *A First Course on Wavelets*, CRC Press, 1996.

[43] J. R. Quinlan, *C4.5: Programs for Machine Learning*, Morgan Kauffman, San Mateo, CA, 1993.

[44]   C. E. Shannon, *"A Mathematical Theory of Communication,"* Bell System Technical Journal, Vol. 27, pp. 379-423, 1948.

[45]   From Comsol, Inc., A web resource, http://www.comsol.com/support/ knowledgebase/120.php?highlight=mesh+generator